

1 Synthetic ozone deposition and stomatal uptake at flux tower sites

2 Jason A. Ducker¹, Christopher D. Holmes¹, Trevor F. Keenan^{2,3}, Silvano Fares⁴, Allen H.
3 Goldstein³, Ivan Mammarella⁵, J. William Munger⁶, Jordan Schnell⁷

4
5 ¹ Department of Earth, Ocean, and Atmospheric Science, Florida State University, Tallahassee,
6 Florida

7 ² Lawrence Berkeley National Laboratory, University of California, Berkeley, California

8 ³ Department of Environmental Science, Policy, and Management, University of California,
9 Berkeley, California

10 ⁴ Council of Agricultural Research and Economics (CREA), Research Centre for Forestry and
11 Wood, Arezzo, Italy.

12 ⁵ Institute for Atmosphere and Earth System Research/Physics, PO Box 68, Faculty of Science,
13 University of Helsinki, Finland

14 ⁶ Department of Earth and Planetary Sciences, Northwestern University, Evanston, Illinois

15
16 ⁷ NOAA Geophysical Fluid Dynamics Laboratory, Princeton, New Jersey

17 18 **Abstract**

19
20 We develop and evaluate a method to estimate O₃ deposition and stomatal O₃ uptake across
21 networks of eddy covariance flux tower sites where O₃ concentrations and O₃ fluxes have not
22 been measured. The method combines standard micrometeorological flux measurements, which
23 constrain O₃ deposition velocity and stomatal conductance, with a gridded dataset of observed
24 surface O₃ concentrations. Measurement errors are propagated through all calculations to
25 quantify O₃ flux uncertainties. We evaluate the method at three sites with O₃ flux measurements:
26 Harvard Forest, Blodgett Forest, and Hyytiälä Forest. The method reproduces 83% or more of
27 the variability in daily stomatal uptake at these sites with modest mean bias (21% or less). At
28 least 95% of daily average values agree with measurements within a factor of two and, according
29 to the error analysis, the residual differences from measured O₃ fluxes are consistent with the
30 uncertainty in the underlying measurements.

31
32 The product, called synthetic O₃ flux or SynFlux, includes 43 FLUXNET sites in the United
33 States and 60 sites in Europe, totaling 926 site-years of data. This dataset, which is now public,
34 dramatically expands the number and types of sites where O₃ fluxes can be used for ecosystem
35 impact studies and evaluation of air quality and climate models. Across these sites, the mean
36 stomatal conductance and O₃ deposition velocity is 0.03-1.0 cm s⁻¹. The stomatal O₃ flux during
37 the growing season (typically April-September) is 0.5-11.0 nmol O₃ m⁻² s⁻¹ with a mean of 4.5
38 nmol O₃ m⁻² s⁻¹ and the largest fluxes generally occur where stomatal conductance is high, rather
39 than where O₃ concentrations are high. The conductance differences across sites can be
40 explained by atmospheric humidity, soil moisture, vegetation type, irrigation, and land

41 management. These stomatal fluxes suggest that ambient O₃ degrades biomass production and
42 CO₂ sequestration by 20-24% at crop sites, 6-29% at deciduous broadleaf forests, and 4-20% at
43 evergreen needleleaf forests in the United States and Europe.

44

45 **1 Introduction**

46

47 Surface ozone (O₃) is toxic to both people and plants. Present-day and recent historical O₃ levels
48 reduce carbon sequestration in the biosphere (Reich and Lassoie, 1984; Guidi et al., 2001; Sitch
49 et al., 2007; Ainsworth et al., 2012), perturb the terrestrial water cycle (Lombardozzi et al., 2012,
50 2015), and cause around \$25 billion in annual crop losses (Reich and Amundson, 1985; Van
51 Dingenen et al., 2009; Avnery et al., 2011; Tai et al., 2014). The basic plant responses to O₃
52 injury are well established from controlled exposure experiments (e.g. Wittig et al., 2009;
53 Ainsworth et al., 2005, 2012; Hoshika et al., 2015) but few datasets are available to quantify O₃
54 fluxes and responses for whole ecosystems or plant functional types that are represented within
55 regional and global biosphere and climate models. The eddy covariance method has been widely
56 used to measure land-atmosphere fluxes of carbon, water, and energy and evaluate their
57 representation in models (Baldocchi et al., 2001; Bonan et al., 2011), but few towers measure O₃
58 fluxes (Munger et al., 1996; Fowler et al., 2001; Keronen et al., 2003; Gerosa et al., 2004;
59 Lamaud et al., 2009; Fares et al., 2010; Stella et al., 2014; Zona et al., 2014). A recent review
60 identified just 78 field measurements of O₃ fluxes over vegetation during the last 4 decades,
61 many lasting just a few weeks (Silva and Heald, 2017). This paper demonstrates a reliable
62 method to estimate O₃ fluxes at 103 eddy covariance flux towers spanning over two decades to
63 enable O₃ impact studies on ecosystem scales.

64

65 The land surface is a terminal sink for atmospheric O₃ due to the reactivity of O₃ with
66 unsaturated organic molecules and the modest solubility of O₃ in water. Surface deposition is
67 20% of the total loss in tropospheric O₃, making it an important control on air pollution (Wu et
68 al., 2007; Young et al., 2013, Kavassalis and Murphy, 2017). This O₃ deposition flux includes
69 stomatal uptake into leaves, where O₃ can cause internal oxidative damage, and less harmful
70 non-stomatal deposition to plant cuticles, stems, bark, soil, and standing water (Fuhrer, 2000;
71 Zhang et al., 2002; Ainsworth et al., 2012). O₃ can also react with biogenic volatile organic
72 compounds, particularly terpenoid compounds, in the plant canopy air and this process is
73 commonly included in non-stomatal deposition (Kurpius and Goldstein, 2003). The deposition
74 flux (mol O₃ m⁻² s⁻¹) can be described as:

$$75 \quad F_{O_3} = v_d n (\chi - \chi_0) = v_d n \chi \quad (1)$$

76 where χ and χ_0 are the O₃ mole fractions (mol mol⁻¹) in the atmosphere and at the surface,
77 respectively, n is the molar density of air (mol m⁻³), and v_d is a deposition velocity (m s⁻¹) that
78 expresses the net vertical O₃ transport between the height where χ is measured and the surface.
79 F_{O_3} is defined positive for flux towards the ground. Eq. 1 reasonably assumes that $\chi_0 = 0$ because
80 terrestrial surfaces have abundant organic compounds that react with and destroy O₃. The

81 deposition velocity can be decomposed into resistances (s m^{-1}) for aerodynamic transport (r_a),
82 diffusion in the quasi-laminar layer (r_b), stomatal uptake (r_s), and non-stomatal deposition (r_{ns})
83 (Wesely, 1989):

$$84 \quad v_d^{-1} = r_a + r_b + (r_s^{-1} + r_{ns}^{-1})^{-1}. \quad (2)$$

85 For stomatal and non-stomatal processes, the rates are often expressed as conductances (m s^{-1}),
86 which are the inverse of the resistances: $g_s = r_s^{-1}$ and $g_{ns} = r_{ns}^{-1}$. The sum of stomatal and non-
87 stomatal conductances is the vegetation canopy conductance, $g_c = g_s + g_{ns}$. The stomatal O_3
88 flux is the portion of F_{O_3} that enters the stomata, and can be described as:

$$89 \quad F_{s,\text{O}_3} = F_{\text{O}_3} g_s (g_s + g_{ns})^{-1} = v_d n \chi g_s (g_s + g_{ns})^{-1}. \quad (3)$$

90
91 To construct the synthetic O_3 flux, or SynFlux, we use measurements of O_3 concentration and
92 standard eddy covariance flux measurements to derive nearly all of the terms in Eqs. 1-3 from
93 surface observations, using some additional information from remote sensing and models. This
94 enables the estimation of F_{O_3} and F_{s,O_3} , as described in Sect. 2. Sect. 3 evaluates the method
95 against observations at three sites that measure F_{O_3} and examines the importance of stomatal and
96 non-stomatal deposition. Sect. 4 uses SynFlux to assess the spatial patterns of O_3 uptake to
97 vegetation and to compare flux-based metrics of O_3 damage with concentration-based metrics.
98 Finally, we discuss the strengths, limitations, and implications of our approach in Sect. 5.

99

100 **2 Data sources and methods**

101

102 **2.1 SynFlux: synthetic O_3 flux**

103

104 The FLUXNET2015 dataset (Pastorello et al., 2017) aggregates measurements of land-
105 atmosphere fluxes of CO_2 , H_2O , momentum, and heat at sites around the world
106 (<http://fluxnet.fluxdata.org/data/fluxnet2015-dataset>, accessed 24 February 2017). Measurements
107 are made with the eddy covariance method on towers above vegetation canopies (Baldocchi et
108 al., 2001; Anderson et al., 1984; Goldstein et al., 2000) with consistent gap-filling (Reichstein et
109 al., 2005; Vuichard and Papale, 2015) and quality control across sites (Pastorello et al., 2014).
110 Flux and meteorological quantities are reported in half hour intervals. We analyze data from all
111 sites in the United States and Europe in the FLUXNET2015 Tier 1 dataset. This analysis is
112 restricted to the US and Europe because these regions have dense O_3 monitoring networks,
113 described below. There are 103 sites meeting these criteria, all listed in Table S1 with references
114 to full site descriptions. Three of these sites—Blodgett Forest, Harvard Forest, and Hyytiälä
115 Forest—measure O_3 flux with the eddy covariance method, which we will use in Sect. 3 to
116 evaluate our methods.

117

118 SynFlux aims to constrain O_3 deposition and stomatal uptake as much as possible from measured
119 water, heat and momentum fluxes, in contrast to other methods (Finkelstein et al., 2000; Mills et
120 al. 2011; Schwede et al., 2011; Yue et al., 2014) that rely more heavily on atmospheric models or

121 parameterizations of stomatal conductance. From the eddy covariance measurements, we derive
122 the resistance components of Eq. 2 using methods similar to past studies (Kurpius and Goldstein,
123 2003; Gerosa et al., 2005; Fares et al., 2010). The aerodynamic and quasi-laminar layer
124 resistances (r_a and r_b , respectively) are derived from measured wind speed, friction velocity, and
125 fluxes of sensible and latent heat every half hour using Monin-Obukhov similarity theory
126 (Foken, 2017). The stomatal conductance for O_3 (g_s) is derived from the measured water vapor
127 flux and meteorological data every half hour with the inverted Penman-Monteith equation
128 (Monteith, 1981; Gerosa et al., 2007). Supplement S1 provides further details of the resistance
129 and conductance calculations. Some studies instead calculate g_s from gross primary productivity
130 (Lamaud et al., 2009; El-Madany et al., 2017), but that method is less widely used than the
131 Penman-Monteith approach adopted here. The Penman-Monteith method of calculating stomatal
132 conductance has been successfully applied across FLUXNET sites previously (Novick et al.,
133 2016; Knauer et al., 2017; Medlyn et al., 2017; Lin et al., 2018). Those studies and others caution
134 that, since evapotranspiration measurements include evaporation from ground, the stomatal
135 conductance could be overestimated. While there are methods for quantifying and removing the
136 evaporative fraction of evapotranspiration from eddy covariance data (Wang et al., 2014; Zhou et
137 al., 2016; Scott and Biederman, 2017), a more common approach is to restrict analysis to
138 conditions when transpiration dominates. We follow this second approach, analyzing only
139 daytime data during the growing season, and use filtering criteria similar to Knauer et al. (2017).
140 We define daytime as sun elevation angle above 4° and the growing season as days when gross
141 primary productivity (GPP) exceeds 20% of the annual maxima in GPP. To avoid complications
142 to the Penman-Monteith equation from wet canopies, we exclude times when dew may be
143 present ($RH > 80\%$), and days with precipitation ($> 5\text{mm}$). We also exclude the top and bottom
144 1% of g_s values, which include many unrealistic outliers (e.g. $|g_s| > 0.5 \text{ m s}^{-1}$). Figure 1 shows
145 the mean stomatal conductance during the growing season at all sites.

146
147 The terms in Eqs. 1-3 that cannot be derived from FLUXNET2015 measurements are O_3 mole
148 fraction and non-stomatal conductance. The O_3 mole fraction is taken from a gridded dataset of
149 hourly O_3 measurements that spans the contiguous United States and Europe (Schnell et al.,
150 2014). This dataset has 1° spatial resolution, so some differences from measured O_3 abundances
151 at individual sites are inevitable. Schnell et al. (2014) estimated these errors to be 6-9 ppb (rms)
152 or about 15% of summer mean O_3 in the US and similar in Europe. Figure 2 shows that the
153 daytime gridded O_3 concentrations correlate well with observations at three flux tower sites
154 where O_3 was measured ($R^2 = 0.63-0.87$) and have modest negative bias (5-10 ppb, -12 to -
155 28%), consistent with the accuracy reported by Schnell et al. (2014). We use the Zhang et al.
156 (2003) parameterization of non-stomatal conductance, which accounts for O_3 deposition to leaf
157 cuticles and ground and was developed from measurements in the eastern United States. The
158 parameterization requires leaf-area index, which we take from satellite remote sensing (Claverie
159 et al., 2014; 2016), snow depth, which we take from MERRA2 reanalysis (GMAO, 2015; Gelaro
160 et al., 2017), and standard meteorological data provided by FLUXNET2015. Uncertainties in

161 these variables are described in Sect. 2.4. Performance of the non-stomatal parameterization is
162 examined in Sect. 3.2.

163
164 Figure 3 shows the stomatal O₃ flux at each site calculated with Eq. 3, then averaged over the
165 growing season. Figure S1 shows the corresponding total O₃ flux (Eq. 1). We refer to these
166 products as the “synthetic” total O₃ flux ($F_{O_3}^{syn}$) and synthetic stomatal O₃ flux (F_{s,O_3}^{syn}). Superscript
167 “syn” distinguishes these synthetic quantities from the observed total O₃ flux ($F_{O_3}^{obs}$) and
168 observation-derived stomatal O₃ flux (F_{s,O_3}^{obs}), which are only available at a few sites. Together,
169 we refer to $F_{O_3}^{syn}$ and F_{s,O_3}^{syn} as SynFlux. In total, the measurements required to calculate F_{s,O_3}^{syn} are
170 O₃ mole fraction, sensible and latent heat fluxes, friction velocity, temperature, pressure,
171 humidity, canopy height, and leaf area index. There are 43 sites in the US and 60 sites in Europe
172 within the FLUXNET Tier 1 database with sufficient measurements to calculate F_{s,O_3}^{syn} .

173
174

175 **2.2 Observed O₃ flux**

176
177 We evaluate SynFlux and its inputs at three sites where O₃ flux measurements are available:
178 Harvard Forest, Massachusetts, United States (Munger et al., 1996); Blodgett Forest, California,
179 United States (Fares et al., 2010); and Hyytiälä Forest, Finland (Keronen et al., 2003;
180 Mammarella et al., 2007; Rannik et al., 2009). These forest sites sample a range of
181 environmental and ecosystem conditions summarized in Table 1. All three sites have at least 6
182 years of half-hourly or hourly flux measurements. Two sites are evergreen needleleaf forests
183 (Blodgett and Hyytiälä), while one is a deciduous broadleaf forest containing some scattered
184 stands of evergreen needleleaf trees (Harvard). Climate also differs across these sites. Blodgett
185 Forest has a Mediterranean climate with cool, wet winters and hot, dry summers. Hyytiälä and
186 Harvard Forests have cold winters and wetter summers, with Harvard Forest being the warmer of
187 the two.

188
189 Harvard Forest water vapor flux measurements were recalibrated for this work based on
190 matching water vapor mixing ratio measured by the flux sensor to levels calculated from ambient
191 relative humidity and air temperature, resulting in a 30% increase in evapotranspiration during
192 the 1990s and no change since 2006. In addition, we remove sub-canopy evaporation from the
193 measured water vapor flux before the Penman-Monteith calculation. Based on past
194 measurements at these sites, the sub-canopy fraction of evapotranspiration is 20% at Hyytiälä
195 Forest, 10% at Harvard Forest in summer (Moore et al., 1996; Launiainen et al., 2005). We are
196 unable to make this correction at all FLUXNET sites since water vapor flux is typically
197 measured only above canopy.

198

199 At these three sites, observation-derived v_d , g_{ns} , and F_{s,O_3} can be derived from the F_{O_3}
 200 measurements with methods that differ slightly from Sect. 2.1. O_3 deposition velocity is inferred
 201 from measurements of O_3 concentration and flux via $v_d = F_{O_3}(n\chi)^{-1}$. Resistance or
 202 conductance terms r_a , r_b , and g_s are calculated as described in Sect. 2.1, then both canopy and
 203 non-stomatal conductance are derived from observations via $g_c = (v_d^{-1} - r_a - r_b)^{-1}$ and $g_{ns} =$
 204 $g_c - g_s$, respectively. With those values, Eq. 3 gives the observation-derived stomatal O_3 flux.
 205 Synthetic and observation-derived stomatal O_3 fluxes are both calculated with Eq. 3 and use the
 206 same observation-derived g_s , r_a , and r_b , but different values of g_{ns} , v_d , and O_3 mole fraction.

207
208

209 **2.3 Gap filling for friction velocity**

210

211 The FLUXNET2015 dataset uses gap filling for most flux and meteorological measurements
 212 (Vuichard and Papale, 2015), but not for friction velocity (u_*), which is required to calculate v_d
 213 and F_{s,O_3}^{syn} . Filling this one variable would significantly reduce the fraction of missing data in our
 214 analysis. Monin-Obukhov similarity theory predicts that friction velocity is proportional to wind
 215 speed in the surface layer, for a given roughness length and stability regime (Foken, 2017). On
 216 this basis, we regress the available friction velocity measurements against wind speed and net
 217 radiation (a proxy for stability) separately for each site and month (a proxy for vegetation
 218 roughness). This gap filling was possible at 91 sites that report net radiation measurements.

219

220 The predicted friction velocities from the regression model are correlated with available
 221 observations ($R^2 > 0.5$) and have minimal mean bias ($\pm 10\%$) at 85 out of 91 eligible sites (Fig.
 222 S3), with most sites (63 out of 91) showing strong correlations ($R^2 > 0.7$). At the remaining 6
 223 sites with lower regression model performance ($R^2 < 0.5$) we do not use u_* gap-filling. The
 224 u_* gap filling increases the number of F_{s,O_3}^{syn} estimates by 1-20%. Time periods with u_* gaps have
 225 no significant bias in meteorological conditions (e.g. mean wind speed, radiation, energy fluxes)
 226 compared to periods with u_* measurements. As a result, the differences in monthly mean F_{s,O_3}^{syn}
 227 with and without gap filling are small (10% rms). So, although the u_* gap filling is a potential
 228 source of uncertainty, the F_{s,O_3}^{syn} estimates are robust. The following analysis will use the gap-
 229 filled data, but our results do not change in any meaningful way if we use the unfilled data.

230

231 **2.4 Error analysis, averaging, and numerical methods**

232

233 We quantify the errors in $F_{O_3}^{syn}$, F_{s,O_3}^{syn} , and all other calculated variables from the measurement
 234 uncertainties using standard techniques for propagation of errors through all equations (see
 235 Supplement S2). This method provides the uncertainty, quantified as standard deviation, of each
 236 variable in each half hour interval. The error analysis reveals that F_{s,O_3}^{syn} and other derived
 237 quantities have uncertainties that change from hour to hour by two orders of magnitude (Fig. S2).

238 In addition, many extreme values of F_{s,O_3}^{syn} , g_s , and other variables have very large uncertainties.
239 We retain these outliers in our analysis and use the error analysis to appropriately reduce their
240 influence on averages and other statistics, as described below, without discarding data.

241
242 The FLUXNET2015 dataset contains error estimates for sensible and latent heat measurements.
243 We use these reported values in the error analysis. Where uncertainties in these fluxes are
244 missing, we fill the gaps using a linear regression of available flux errors against flux values for
245 that site. For friction velocity, the uncertainty is the prediction error in the linear model used for
246 gap filling (Sect. 2.3). Based on expert judgment, the standard deviation of O_3 mole fraction is
247 set to 20%, pressure to 0.5 hPa, temperature to 0.5 K, relative humidity to 5%, and canopy height
248 to the lesser of 15% or 2 m. For remotely sensed leaf area index, the uncertainty is $1.1 \text{ m}^2 \text{ m}^{-2}$ for
249 all vegetation types (Claverie et al., 2013; 2016). Snow depth uncertainty in MERRA2 is 0.08 m
250 (Reichle et al., 2017). The Zhang et al. (2003) g_{ns} parameterization has 5 vegetation-specific
251 parameters and all are assigned 50% standard deviation. Zero error is assumed for the flux tower
252 height. Based on these inputs, the median relative uncertainty in F_{s,O_3}^{syn} is 44%, but it rises to
253 several hundred percent for some half-hour intervals. The error analysis shows that most of the
254 uncertainty in F_{s,O_3}^{syn} derives from uncertainty in the latent heat flux measurement.

255
256 Daily and monthly averages of F_{s,O_3}^{syn} and other quantities are constructed in stages. We first
257 calculate a mean diurnal cycle for the day or month by pooling measurements during each hour
258 in a maximum likelihood estimate, a weighted average that accounts for the uncertainty in each
259 measurement. The maximum likelihood estimate is appropriate when combining values from the
260 same distribution, which is expected to apply for measurements within a particular hour, but not
261 across hours of the day. We then average across hours with an unweighted mean to calculate the
262 daily or monthly value. For the daily averages, there are 1-2 observations within each hour. For
263 the monthly averages, there are typically 30-60 in each hour of the day. We calculate seasonal
264 averages with an unweighted mean of monthly values. Uncertainties are propagated through each
265 stage of these averages, as detailed in Supplement S2. We compared averages with and without
266 uncertainty weighting. The uncertainty-weighted averages tend to be smaller and less variable
267 than unweighted averages because the error propagation identifies when outliers and large values
268 have greater uncertainty. For example, the monthly values of g_c derived from observations at
269 Harvard Forest are $0.57 \pm 0.11 \text{ cm s}^{-1}$ with uncertainty weighting and $0.68 \pm 0.17 \text{ cm s}^{-1}$ without.
270 Our discussion focuses on uncertainty-weighted daily averages of daytime data.

271 Analyses are performed in Python 3.5 with NumPy, Pandas, PySolar, and Statsmodels (Reda and
272 Andreas, 2005; Van Der Walt et al., 2006; McKinney, 2010; Seabold et al., 2010). We quantify
273 linear relationships between variables using the coefficient of determination (R^2), a parametric
274 slope estimator (standard major axis or SMA, Warton et al. 2006) and a non-parametric slope
275 estimator (Thiel-Sen slope, Sen, 1968), which is more robust against outliers.

276

277 2.5 Data availability

278

279 The SynFlux dataset produced in this work is available at

280 <https://doi.org/10.5281/zenodo.1402054>. The dataset includes synthetic stomatal and total O₃

281 fluxes, O₃ concentrations, O₃ deposition velocity, canopy conductance, stomatal conductance,

282 and all of their propagated uncertainties. Monthly mean values are provided with and without u_*

283 gap filling, for 103 sites totaling 926 site-years.

284

285

286 3 SynFlux evaluation

287

288 3.1 Evaluation of synthetic fluxes

289

290 Figure 4 compares daily daytime averages of synthetic F_{s,O_3}^{syn} to observation-derived F_{s,O_3}^{obs} . F_{s,O_3}^{syn}

291 and F_{s,O_3}^{obs} are calculated from the same observation-derived stomatal conductance (g_s) and

292 aerodynamic resistances (r_a and r_b) but differ in the O₃ mole fraction and non-stomatal

293 conductance (g_{ns}) that they use (see Sect. 2.1 and 2.2). At all three sites, F_{s,O_3}^{syn} is strongly

294 correlated with measured values ($R^2 = 0.83-0.93$). The mean and median biases are -16 to -21%

295 and at least 95% of F_{s,O_3}^{syn} values agree with measurements within a factor of 2. The majority of

296 F_{s,O_3}^{syn} values lie near the 1:1 line with F_{s,O_3}^{obs} and the slopes (0.71 to 0.85) reflect this. The half-

297 hourly or hourly measured and synthetic flux still have some outliers (Fig. S2), but the error

298 analysis reveals that many of the outlying points have large uncertainties. For 98% of points, the

299 differences between F_{s,O_3}^{syn} and F_{s,O_3}^{obs} are less than the 95% confidence interval derived from the

300 error analysis (two-sided t test). Thus, the errors in F_{s,O_3}^{syn} are consistent with the propagated

301 uncertainty in the observations. The half hourly F_{s,O_3}^{syn} values perform similarly well against

302 observations (Fig. S4), but our analysis focuses on averages. The performance of daily F_{s,O_3}^{syn} is

303 partially due to resolving the seasonal cycle. If we subtract the mean seasonal cycle from both

304 synthetic and observation-derived daily F_{s,O_3} , the residual correlation is $R^2 = 0.5-0.7$ (versus 0.9

305 with seasonal cycle included). This represents the skill of SynFlux at reproducing within-month

306 and interannual variability. Overall, these results suggest that synthetic F_{s,O_3}^{syn} is a reliable estimate

307 of stomatal O₃ uptake into plants that can be used at flux tower sites without O₃ measurements.

308

309 The measurements also enable us to evaluate synthetic total deposition, $F_{O_3}^{syn}$, and synthetic O₃

310 deposition velocity, v_d^{syn} , although these are less relevant to ecosystem impacts than stomatal

311 uptake, F_{s,O_3}^{syn} . For daily averages, Figure S5 shows that $F_{O_3}^{syn}$ bias (-13 to $+65\%$), slope (0.3-1.4),

312 and R^2 (0.05-0.43) are all worse than for F_{s,O_3}^{syn} . The daily v_d^{syn} performance is similar (Fig. S6,

313 bias: -26 to $+41\%$, slope: 0.3 - 1.1 , R^2 : 0.16 - 0.37). Monthly averages of v_d^{syn} and $F_{\text{O}_3}^{\text{syn}}$ both
314 improve the correlation to observations ($R^2 \sim 0.12$ - 0.54). The reasons for the better performance
315 of $F_{s,\text{O}_3}^{\text{syn}}$ compared to $F_{\text{O}_3}^{\text{syn}}$ can be derived from Eq. 3. The canopy resistance for O_3 is normally
316 much greater than the quasi-laminar layer and aerodynamic resistances, meaning $r_c \gg$
317 r_a and $r_c \gg r_b$, often by a factor of 3 - 10 . Therefore, the O_3 deposition velocity is approximately
318 $v_d \approx r_c^{-1} = g_c$. Under these conditions, Eq. 1 simplifies to $F_{\text{O}_3} \approx n\chi(g_s + g_{ns})$ and Eq. 3
319 simplifies to $F_{s,\text{O}_3} \approx n\chi g_s$. While g_s is calculated from measured H_2O fluxes, g_{ns} comes from a
320 parameterization, which inevitably introduces error into g_{ns} and $F_{\text{O}_3}^{\text{syn}}$. However, $F_{s,\text{O}_3}^{\text{syn}}$ has little
321 sensitivity to g_{ns} regardless of whether stomatal or non-stomatal conductance is larger. We
322 confirm this insensitivity in tests where the parameterized g_{ns} value is doubled at ten sites. The
323 hourly $F_{s,\text{O}_3}^{\text{syn}}$ values change only 3 - 8% . Since $F_{s,\text{O}_3}^{\text{syn}}$ has little sensitivity to g_{ns} or its errors, it can
324 be calculated more accurately than $F_{\text{O}_3}^{\text{syn}}$, as seen when comparing Figures 4 and S4. Despite its
325 larger errors, the means of $F_{\text{O}_3}^{\text{syn}}$ and v_d^{syn} are within 50% of the observed value at two sites and
326 within a factor of 2 at all, which may be useful for some applications, given the scarcity of prior
327 F_{O_3} measurements and observation-derived estimates of v_d .

328
329

330 **3.2 Stomatal and non-stomatal deposition**

331

332 Figure 5 shows the seasonal cycles of observation-derived O_3 deposition velocity and its
333 important components at the three study sites with O_3 flux measurements. For low or moderately
334 reactive gases like O_3 , canopy resistance is typically greater than aerodynamic or quasi-laminar
335 layer resistance, so it controls the overall deposition velocity. At these three sites, deposition
336 velocity is lowest in winter (0.1 - 0.2 cm s^{-1}) and highest in summer (0.5 - 0.6 cm s^{-1}). Stomatal
337 conductance peaks during warm and wet months, which explains most of this seasonal variation,
338 except at Blodgett Forest as discussed below. Traditionally, stomatal conductance was thought to
339 exceed non-stomatal conductance during the growing season at most vegetated sites (Wesely,
340 1989; Zhang et al., 2003), although this has been challenged more recently (Altimir et al., 2006;
341 Stella et al., 2011; Wolfe et al., 2011; Plake et al., 2015). At both Harvard and Hyytiälä Forests,
342 the mean stomatal conductance (0.2 - 0.6 cm s^{-1}) is 1.5 - 6 times larger than non-stomatal
343 conductance (0.08 - 0.2 cm s^{-1}) during the growing season, so about 60 - 90% of O_3 deposition
344 occurs through stomatal uptake. At Blodgett, non-stomatal conductance slightly exceeds stomatal
345 conductance in summer (0.4 vs. 0.3 cm s^{-1}). The fast non-stomatal deposition is explained by O_3
346 reacting with biogenic terpenoid emissions below the flux measurement height (Kurpius and
347 Goldstein, 2003; Fares et al., 2010). As documented in past work, these biogenic emissions
348 depend strongly on temperature and light and have a large seasonal cycle with maxima in
349 summer and minima in winter, so stomatal uptake is generally $< 50\%$ of O_3 deposition at

350 Blodgett in the summer but > 70% in winter (Kurpuis and Goldstein, 2003; Fares et al., 2010;
351 Wolfe et al. 2011).

352
353 A recent analysis of O₃ flux measurements at Harvard Forest suggests that non-stomatal
354 deposition averages 40% of daytime O₃ deposition during summer months, with a range of 20-
355 60% across years (Clifton et al., 2017). Our analysis of the same site does not support such a
356 large role for non-stomatal deposition at this site in summer. For each year, we calculate summer
357 daytime means of g_s and g_c by averaging the June-September values, then calculate the non-
358 stomatal fraction of deposition ($1 - g_s/g_c$). Averaged across years 1993-2000, we find that 8%
359 of daytime O₃ deposition is non-stomatal during the summer, with a range of -33% to 34%
360 across years. Negative fractions mean that stomatal conductance is large enough to explain all O₃
361 deposition. A large negative non-stomatal fraction (-33%) occurs in only one year (1996) and no
362 other year is less than -11%, which is within uncertainty of 0% (2σ) according to the error
363 propagation. Despite the small or zero non-stomatal fraction found here, our results continue to
364 support the large year-to-year variability of this fraction reported by Clifton et al. (2017). The re-
365 calibrated latent heat flux measurements are the main reason that our results differ from prior
366 work and Supplement S3 provides further details. At Hyytiälä Forest, our results are consistent
367 with prior work that found that the non-stomatal deposition is 26% to 44% of daytime O₃
368 deposition during the growing season (Rannik et al., 2012). Nevertheless, non-stomatal
369 deposition equals or exceeds stomatal uptake where there are large terpene emissions (e.g.
370 Blodgett) and at some other temperate sites that probably lack large biogenic emissions (Fowler
371 et al., 2001; Cieslik, 2004; Lamaud et al., 2009; Stella et al., 2011; El-Madany et al., 2017). We
372 also examined interannual variation in O₃ deposition velocity. We find that the mean summer
373 daytime v_d is 0.40-0.68 cm s⁻¹ at Harvard Forest, 0.42-0.65 cm s⁻¹ at Blodgett Forest, and 0.43-
374 0.51 cm s⁻¹ at Hyytiälä. This range for Harvard Forest is somewhat smaller than other recent
375 work (0.5-1.2 cm s⁻¹; Clifton et al., 2017) because of the uncertainty-weighted averages used here
376 (Sect. 2.4).

377
378 The data here also provide an opportunity to evaluate the parameterization of non-stomatal
379 conductance (Zhang et al., 2003). The parameterized g_{ns} has similar mean to observation-
380 derived values in summer at Harvard Forest (0.16 vs. 0.12 cm s⁻¹) and Hyytiälä (0.15 vs. 0.25 cm
381 s⁻¹). At Blodgett Forest, the parameterized g_{ns} is about half of observation-derived g_{ns} in
382 summer, but this is not surprising since the parameterization does not account for O₃ reactions
383 with biogenic volatile organic compounds (BVOC), which are known to be important at this site
384 (Fares et al., 2010). In winter, however, the parameterized g_{ns} values at Blodgett Forest are
385 similar to observations (0.10 vs. 0.08 cm s⁻¹). The parameterization is therefore able to roughly
386 predict mean non-stomatal conductance in the absence of major BVOC emissions. Nevertheless,
387 the parameterization reproduces almost none of the daily variability of g_{ns} at any site ($R^2 < 0.1$,
388 Fig. S7). This corroborates the recent field assessment that non-stomatal conductance is a weak
389 point of most current dry deposition algorithms (Wu et al., 2018). We attempted, unsuccessfully,

390 to use BVOC emissions from the MEGAN biogenic emission model (Guenther et al., 2012) to
391 improve the g_{ns} parameterization, but the correlations between compounds that react fastest with
392 O_3 (monoterpenes and sesquiterpenes) and the observation-derived daily mean g_{ns} were poor (R^2
393 ≤ 0.15). On that basis, $F_{O_3}^{syn}$ may also underestimate total O_3 deposition at other sites with high
394 monoterpene and sesquiterpene emissions, such as warm-weather pine forests, but F_{s,O_3}^{syn} should
395 retain its quality everywhere.

396

397 4 SynFlux applications

398

399 4.1 Spatial patterns of synthetic fluxes

400

401 Across the 43 sites in the US shown in Fig. 3, mean F_{s,O_3}^{syn} during the growing season ranges from
402 0.5 to 11.0 $nmol O_3 m^{-2} s^{-1}$ with an average of 4.4 $nmol O_3 m^{-2} s^{-1}$. The highest F_{s,O_3}^{syn} generally
403 occurs in the Midwest (5-9 $nmol O_3 m^{-2} s^{-1}$ in Wisconsin, Michigan, Nebraska, Ohio) due to its
404 moderate O_3 concentrations (Fig. S6) and moisture levels, which promotes stomatal conductance
405 (Fig. 1). The Western US has higher average O_3 concentrations, but generally lower moisture
406 and stomatal conductance, especially the Southwest US, so F_{s,O_3}^{syn} (0-4 $nmol O_3 m^{-2} s^{-1}$) is mostly
407 lower than the Midwest. Land cover, land management, and plant types can drive large
408 differences in F_{s,O_3}^{syn} between nearby sites, even when O_3 concentrations and meteorology are
409 similar. For example, three Nebraska sites are all crop fields and O_3 concentrations are nearly
410 identical, but two irrigated fields have higher stomatal conductance and higher F_{s,O_3}^{syn} than the
411 nearby rainfed field (6.2 vs. 4.8 $nmol O_3 m^{-2} s^{-1}$). Two sites in central California have high g_s and
412 F_{s,O_3}^{syn} compared to surrounding sites due to irrigation and naturally wet soil in the California
413 Delta. A combination of topography and climate is also an important factor in California: forest
414 sites in the Sierra Nevada mountains have lower g_s and F_{s,O_3}^{syn} than the lowland crops and wetland
415 grasses. In Oregon, an evergreen needleleaf site regrowing after a fire has higher g_s and F_{s,O_3}^{syn}
416 than two older forest stands nearby. The differences between 9 Wisconsin forest sites, however,
417 are mostly due to different years of data at each site combined with interannual variability in
418 F_{s,O_3}^{syn} ; fluxes at these sites are similar in overlapping years.

419

420 Variability across the 60 sites in Europe is controlled by similar factors. Stomatal uptake ranges
421 from 1.4 to 9.6 $nmol O_3 m^{-2} s^{-1}$, with an average of 4.7 $nmol O_3 m^{-2} s^{-1}$ (Fig. 3). The
422 Mediterranean region has high O_3 concentrations (Fig. S8), but generally low stomatal
423 conductance due to the dry climate (Fig. 1). Within this region, vegetation type explains broad
424 patterns. Shrub sites in Spain, France, and Sardinia have very low g_s ($\sim 0.15 cm s^{-1}$) so F_{s,O_3}^{syn} is
425 low (1-3 $nmol O_3 m^{-2} s^{-1}$), while most of the sites in mainland Italy are broadleaf and evergreen
426 forests that have slightly greater g_s ($\sim 0.2-0.4 cm s^{-1}$) and F_{s,O_3}^{syn} (3-6 $nmol O_3 m^{-2} s^{-1}$), despite

427 similar climate and O₃. In central and northern Europe, temperate climate promotes higher
 428 stomatal conductance while O₃ concentrations remain modest throughout the growing season.
 429 The largest F_{s,O_3}^{syn} is 9.8 nmol O₃ m⁻² s⁻¹ at a deciduous broadleaf forest in Switzerland, while
 430 nearby evergreen forests, cereal crops, and grasslands all have lower fluxes (6-8 nmol O₃ m⁻² s⁻¹).
 431 While Finland has generally low F_{s,O_3}^{syn} of 2-5 nmol O₃ m⁻² s⁻¹, the high end of this range is similar
 432 to rural sites in Germany, illustrating that O₃ can impact remote ecosystems with high stomatal
 433 conductance, even where O₃ concentrations are low.

434
 435 Table 2 quantifies SynFlux, O₃ deposition velocity, and conductance for each plant functional
 436 type. Wetlands, crops, and forests have the highest average F_{s,O_3}^{syn} , which is about two times
 437 higher than woody savanna or shrublands, the vegetation types with the lowest F_{s,O_3}^{syn} . At wetland
 438 sites, g_s and F_{s,O_3}^{syn} could be overestimated due to evaporation of surface water (Sect. 2.1), but any
 439 error is likely modest because our estimates of stomatal conductance at these sites (0.48 ± 0.16
 440 cm s⁻¹; Table 2) are reasonable for wetland vegetation (up to 1 cm s⁻¹; Drake et al., 2013). The
 441 vegetation types rank in the same order for stomatal conductance, again showing stomata as the
 442 main control on O₃ uptake into vegetation. Stomatal uptake exceeds non-stomatal uptake for all
 443 plant functional types except woody savanna and shrubland. O₃ deposition velocities reported in
 444 Table 2 fall within the ranges of past literature, as reviewed by Silva and Heald (2017).
 445 However, while Silva and Heald found that the mean deposition velocity was greater over
 446 deciduous forests than coniferous forests, crops, or grass, we do not. Rather, we find that
 447 variability between sites within each of these categories is large, having a standard deviation
 448 about 30% of the multi-site mean.

449 4.2 Metrics for O₃ damage to plants

451
 452 Since O₃ injures plants mainly by internal oxidative damage after entering the leaves through
 453 stomata, the most physiological predictor of plant injuries is the cumulative uptake of O₃ (CUO,
 454 Reich, 1987; Fuhrer, 2000; Karlsson et al., 2004; Cieslik, 2004; Matyssek et al., 2007). CUO is
 455 defined as the cumulative stomatal O₃ flux exceeding a threshold flux Y that can be detoxified by
 456 the plant, integrated over a period of time:

$$457 \quad CUOY = \sum_i H(F_{s,O_3,i} - Y)(F_{s,O_3,i} - Y) \Delta t_i.$$

458 Here, $H(x)$ is the Heaviside step function and Δt_i is the time elapsed during measurement of
 459 $F_{s,O_3,i}$. The sum is carried out over time i in the growing season, which we define based on GPP
 460 (Sect 2.1), The detoxification threshold varies across vegetation types, even among related
 461 species (Karlsson et al., 2004, Büker et al., 2015), and thresholds for specific FLUXNET sites
 462 are generally unknown. As a compromise, we calculate CUO, with Y=0, and also CUO3, with Y
 463 = 3 nmol O₃ m⁻² s⁻¹, which has been suggested as a reasonable generic threshold (Mills et al.,

464 2011). CUO is always greater than CUO3, but the sites with high CUO tend to also have high
465 CUO3, so their spatial patterns are similar (Fig. S8).

466

467 While CUO is a physiological dose, concentration-based metrics remain common for assessing
468 ozone impacts because they are easier to measure. Concentration-based metrics quantify O₃ in
469 ambient air irrespective of whether that O₃ enters leaves. These metrics follow the general form

470

$$M = \sum_i w(\chi_i) (\chi_i - \chi_c) \Delta t_i$$

471 where $w(\chi)$ is a weighting function applied to the O₃ mole fraction χ , and χ_c is a constant. Like
472 CUO, the sum is usually over time i during the growing season. Three of the most common
473 concentration-based O₃ metrics are the mean O₃ concentration, the accumulated concentration
474 over a threshold of 40 ppb (AOT40; UNECE, 2004), and the sigmoidal-weighted index (W126;
475 Lefohn and Runeckles, 1987). For mean, $w(\chi) = (\sum \Delta t_i)^{-1}$ and $\chi_c = 0$. For AOT40, $w(\chi) =$
476 $H(\chi - \chi_c)$ and $\chi_c = 40$ ppb. For W126, $w(\chi) = (1 + 4403 \exp(-(126 \text{ ppb}^{-1})\chi))^{-1}$ and $\chi_c =$
477 0. Both AOT40 and W126 use only daytime (8am-8pm) measurements and W126 also takes the
478 maximum value over all 3-month periods during the growing season. The weighting functions
479 for AOT40 and W126 give little or no weight to O₃ concentrations below 40 ppb. In addition,
480 W126 gives increasing weight to concentrations up to about 110 ppb and full weight for higher
481 concentrations based on the understanding that exposure to high O₃ concentrations is more
482 injurious than moderate or low concentrations. Other concentration-based metrics (e.g. SUM60)
483 use other thresholds or weighting functions, but many are strongly correlated with AOT40 or
484 W126 or otherwise qualitatively similar (Paoletti et al., 2007).

485

486 The spatial patterns of AOT40 and W126 closely resemble that of mean O₃ concentration in the
487 US and Europe despite their different weighting functions (Fig. S9). AOT40 and W126 are well
488 correlated with each other across sites ($R^2 = 0.87$) and with mean O₃ mole fraction ($R^2 = 0.76$ and
489 $R^2 = 0.52$ for mean O₃ vs. AOT40 and W126, respectively) despite their different weighting
490 functions. As a result, all of these concentrations-based metrics have similar spatial patterns in
491 the US and Europe. The CUO and CUO3 spatial patterns, however, are similar to F_{s,O_3}^{syn} and
492 distinct from the concentration-based metrics. This illustrates that locations with high AOT40 or
493 W126, like the Southwest US or Mediterranean Europe, can have low CUO.

494

495 Even though concentration-based metrics do not measure the physiological O₃ dose to plants,
496 they can be useful if the metric is proportional to the flux-based dose and injuries. Indeed, many
497 controlled experiments and observational studies have documented correlations between both
498 AOT40 and W126 and either uptake or plant injuries (e.g. Fuhrer et al., 1997; Cieslik, 2004;
499 Musselman et al., 2006; Matyssek et al., 2010). However, many of these studies were carried out
500 at a single site or under conditions where stomatal conductance was relatively steady while O₃
501 concentrations varied, for example by maintaining well-watered soil. When stomatal

502 conductance varies widely, such as between arid and humid climates or seasons, concentration-
503 based metrics may not correlate with stomatal O₃ flux (Mills et al., 2011).

504

505 Figure 6 shows that all of the concentration-based metrics are poorly correlated with CUO across
506 the sites (AOT40: $R^2 = 0.05$, W126: $R^2 = 0.03$, mean O₃: $R^2 = 0.04$). Humidity helps explain some
507 of the scatter in Figure 6. The sites with high concentration-based metrics and low CUO have
508 high vapor pressure deficit (VPD), low stomatal conductance, and are mostly in the western US
509 and Mediterranean Europe. Restricting the analysis to humid sites (VPD < 1.5 kPa) does not
510 improve the correlation ($R^2 \approx 0.05$) and at the arid sites (VPD > 1.6 kPa) the concentration-based
511 metrics are modestly anti-correlated with CUO (AOT40: $R^2 = 0.19$, W126: $R^2 = 0.05$, mean O₃:
512 $R^2 = 0.37$). This result reinforces that concentration-based metrics can misrepresent CUO and
513 plant injuries (Mills et al., 2011).

514

515 From the CUO values in Table 2, we can estimate the range of O₃ impacts on biomass
516 production at the FLUXNET sites. Although species vary in their sensitivity to O₃ (Lombardozzi
517 et al., 2013), several studies suggest that the biomass production of broadleaf and needleleaf
518 trees decreases 0.2 to 1% per mmol O₃ m⁻² of CUO (Karlsson et al., 2004; Wittig et al., 2007;
519 Hoshika et al., 2015). Combining the mean CUO for each plant functional type (Table 2) with
520 these sensitivities, our work implies that O₃ reduces the biomass production at these FLUXNET
521 sites by 6-29% for deciduous broadleaf forests and 4-20% for needleleaf forests. The range
522 represents the spread of reported dose-response sensitivities within each plant type, meaning the
523 least and most O₃-sensitive species. Several broadleaf crops are more sensitive to O₃, with
524 biomass reductions of 1.3-1.6% per mmol O₃ m⁻² of CUO₃ (Mills et al., 2011). That sensitivity
525 implies 20-24% drop in biomass production at FLUXNET crop sites. Some studies have
526 quantified O₃ dose-response relationships with other thresholds $Y = 1.6$ to $6 \text{ nmol O}_3 \text{ m}^{-2} \text{ s}^{-1}$ (e.g.
527 Karlsson et al., 2007; Pleijel et al., 2004, 2014), but the sensitivities have similar magnitude.
528 Fares et al. (2013) also demonstrated 12-19% reduction in gross primary production due to O₃ at
529 some of the same crop and forest FLUXNET sites. Using prognostic models of O₃
530 concentrations and stomatal uptake, several past studies have also suggested that O₃ reduces
531 biomass production and CO₂ sequestration by 4-20% in the US and Europe (Sitch et al., 2007;
532 Wittig et al., 2007; Mills et al., 2011; Yue et al., 2014, 2016; Lombardozzi et al., 2015). Our
533 results support this range of impacts, although some FLUXNET sites and species likely
534 experience greater O₃ injury, but here the CUO is highly constrained from observations and
535 therefore avoids the additional uncertainties of atmosphere-biosphere models.

536

537

538 **5 Conclusions**

539

540 We have demonstrated a method to estimate O₃ fluxes and stomatal O₃ uptake at eddy
541 covariance flux towers wherever regional O₃ monitors exist. The method, called SynFlux,

542 derives stomatal conductance and O₃ deposition velocity from standard eddy covariance
543 measurements and combines them with gridded O₃ concentrations from air quality monitoring
544 networks. We apply this method to the FLUXNET2015 dataset and derive synthetic flux
545 estimates at 43 sites in the United States and 60 sites in Europe, totaling 926 site-years of
546 observations. O₃ deposition measurements have previously only been sporadically available for a
547 few sites around the world, so this work dramatically increases the flux data available for
548 understanding O₃ impacts on vegetation and for evaluating air quality and climate models.

549
550 Three sites with long-term O₃ flux measurements provide an independent test of SynFlux. These
551 comparisons show that daily averages of synthetic stomatal F_{s,O_3}^{syn} correlate well with observation-
552 derived F_{s,O_3}^{obs} ($R^2 = 0.83-0.93$) and have a mean bias under 22% at all sites. At all three sites 95%
553 of the synthetic F_{s,O_3}^{syn} values differ from measurements by a factor of 2 or less. The differences
554 between F_{s,O_3}^{syn} and F_{s,O_3}^{obs} are also consistent with propagated uncertainty in the underlying
555 measurements. Synthetic total deposition, $F_{O_3}^{syn}$, is sensitive to errors in the parameterized non-
556 stomatal conductance, but mean values are still within a factor of 2 of observations. The errors in
557 this dataset are modest compared with differences between observations and regional and global
558 atmospheric chemistry models that are frequently a factor of 2 or more (Zhang et al., 2003;
559 Hardacre et al., 2015; Clifton et al., 2017; Silva and Heald, 2017), illustrating the utility of this
560 dataset for evaluating models and O₃ impacts.

561
562 Across flux tower sites in the US and Europe, F_{s,O_3}^{syn} ranges from 0.5 to 11.0 nmol O₃ m⁻² s⁻¹
563 during the summer growing season. The spatial pattern of F_{s,O_3}^{syn} is mainly controlled by stomatal
564 conductance rather than O₃ concentration. Patterns of stomatal conductance and F_{s,O_3}^{syn} in turn are
565 explained by climate, especially atmospheric and soil moisture, vegetation types, and land
566 management, such as irrigation. O₃ concentration-based metrics (AOT40, W126, mean O₃) have
567 been widely used to evaluate O₃ damages to plants because they are easier and cheaper to
568 measure than the cumulative uptake of O₃ (CUO) into leaves. However, these metrics have very
569 little correlation with CUO ($R^2 \leq 0.05$) across FLUXNET sites. Using dose-response
570 relationships between CUO and biomass reduction, we estimate that O₃ reduces biomass
571 production and carbon uptake by 4-29%, depending on the site and plant type. Unlike most past
572 estimates, which have used prognostic models of O₃ uptake, our assessment of biomass reduction
573 is based on O₃ fluxes that are tightly constrained by observations. To promote further
574 applications in ecosystem monitoring and modeling, the SynFlux dataset is publicly available as
575 monthly averages of F_{s,O_3}^{syn} , $F_{O_3}^{syn}$, O₃ deposition velocity, stomatal conductance, and related
576 variables.

577
578
579

580 **Acknowledgments**

581 This work was supported by the Winchester Fund and by the Council on Research Creativity at
582 Florida State University. Eddy covariance data used here were acquired and shared by the
583 FLUXNET community, including the AmeriFlux and CarboEuropeIP networks. The FLUXNET
584 eddy covariance data processing and harmonization was carried out by the European Fluxes
585 Database Cluster, AmeriFlux Management Project, and Fluxdata project of FLUXNET, with the
586 support of CDIAC and ICOS Ecosystem Thematic Center, and the OzFlux, ChinaFlux and
587 AsiaFlux offices. TFK was supported by the Director, Office of Science, Office of Biological
588 and Environmental Research of the US Department of Energy under Contract DE-AC02-
589 05CH11231 as part of the RUBISCO SFA. The O₃ concentration and flux measurements from
590 Harvard Forest used in this analysis were supported by the National Science Foundation through
591 the LTER program and various programs under the U. S. Department of Energy Office of
592 Science (BER). At Hyytiälä Forest, O₃ concentrations and flux measurements were supported by
593 ICOS-Finland (281255) and Academy of Finland Center of Excellence programme (307331). At
594 Blodgett Forest, O₃ concentrations and flux measurements were supported by ICOS-Finland
595 (281255) and Academy of Finland Center of Excellence programme (307331). The long term O₃
596 concentration and flux measurements from Blodgett Forest used in this analysis were supported
597 by a combination of grants from the Kearney Foundation of Soil Science, the University of
598 California Agricultural Experiment Station, and the U.S. Department of Energy Office of
599 Science (BER), the National Science Foundation Atmospheric Chemistry Program, and the
600 California Air Resources Board. SynFlux data are publicly available at
601 <https://doi.org/10.5281/zenodo.1402054>.
602

603 **References**

604

605 Acosta, M., Pavelka, M., Montagnani, L., Kutsch, W., Lindroth, A., Juszczak, R. and Janouš, D.:
606 Soil surface CO₂ efflux measurements in Norway spruce forests: Comparison between four
607 different sites across Europe — from boreal to alpine forest, *Geoderma*, 192, 295–303,
608 doi:10.1016/j.geoderma.2012.08.027, 2013.

609

610 Ainsworth, E. A. and Long, S. P.: What have we learned from 15 years of free-air CO₂
611 enrichment (FACE)? A meta-analytic review of the responses of photosynthesis, canopy
612 properties and plant production to rising CO₂, *New Phytol.*, 165(2), 351–372,
613 doi:10.1111/j.1469-8137.2004.01224.x, 2005.

614

615 Ainsworth, E. E. a, Yendrek, C. R., Sitch, S., Collins, W. J. and Emberson, L. D.: The effects of
616 tropospheric ozone on net primary productivity and implications for climate change., *Annu. Rev.*
617 *Plant Biol.*, 63(March), 637–61, doi:10.1146/annurev-arplant-042110-103829, 2012.

618

619 Altimir, N., Kolari, P., Tuovinen, J., Vesala, T., Bäck, J., Suni, T., Hari, P., Altimir, N., Kolari,
620 P., Tuovinen, J., Vesala, T. and Bäck, J.: Foliage surface ozone deposition: a role for surface
621 moisture?, *Biogeosciences*, 3, 209–228, <http://doi.org/10.5194/bg-3-209-2006>.

622

623 Ammann, C., Spirig, C., Leifeld, J. and Neftel, A.: Assessment of the nitrogen and carbon budget
624 of two managed temperate grassland fields, *Agric. Ecosyst. Environ.*, 133(3–4), 150–162,
625 doi:10.1016/j.agee.2009.05.006, 2009.

626

627 Anderson, D. E., Verma, S. B. and Rosenberg, N. J.: Eddy correlation measurements of CO₂,
628 latent heat, and sensible heat fluxes over a crop surface, *Boundary-Layer Meteorol.*, 29(3), 263–
629 272, doi:10.1007/BF00119792, 1984.

630

631 Anthoni, P. M., Knohl, A., Rebmann, C., Freibauer, A., Mund, M., Ziegler, W., Kolle, O. and
632 Schulze, E.-D.: Forest and agricultural land-use-dependent CO₂ exchange in Thuringia,
633 Germany, *Glob. Chang. Biol.*, 10(12), 2005–2019, doi:10.1111/j.1365-2486.2004.00863.x, 2004.
634 Aubinet, M., Chermanne, B., Vandenhaute, M., Longdoz, B., Yernaux, M. and Laitat, E.: Long
635 term carbon dioxide exchange above a mixed forest in the Belgian Ardennes, *Agric. For.*
636 *Meteorol.*, 108(4), 293–315, doi:10.1016/s0168-1923(01)00244-1, 2001.

637

638 Avnery, S., Mauzerall, D. L., Liu, J. and Horowitz, L. W.: Global crop yield reductions due to
639 surface ozone exposure: 1. Year 2000 crop production losses and economic damage, *Atmos.*
640 *Environ.*, 45(13), 2284–2296, doi:10.1016/j.atmosenv.2010.11.045, 2011.

641

642 Baldocchi, D.: AmeriFlux US-Tw4 Twitchell East End Wetland, , doi:10.17190/AMF/1246151,
643 2016.

644

645 Baldocchi, D., Falge, E., Gu, L., Olson, R., Hollinger, D., Running, S., Anthoni, P., Bernhofer,
646 C., Davis, K., Evans, R., Fuentes, J., Goldstein, A., Katul, G., Law, B., Lee, X., Malhi, Y.,
647 Meyers, T., Munger, W., Oechel, W., Paw, U. K. T., Pilegaard, K., Schmid, H. P., Valentini, R.,
648 Verma, S., Vesala, T., Wilson, K. and Wofsy, S.: FLUXNET: A new tool to study the temporal

649 and spatial variability of ecosystem-scale carbon dioxide, water vapor, and energy flux densities,
650 *Bull. Am. Meteorol. Soc.*, 82(11), 2415–2434, doi:10.1175/1520-0477, 2001.

651

652 Baldocchi, D., Chen, Q., Chen, X., Ma, S., Miller, G., Ryu, Y., Xiao, J., Wenk, R. and Battles, J.:
653 The dynamics of energy, water, and carbon fluxes in a blue oak (*Quercus douglasii*) savanna in
654 California, *Ecosyst. Funct. Savannas*, 1, 135–151, doi:10.1201/b10275-10, 2010.

655

656 Berbigier, P., Bonnefond, J.-M. and Mellmann, P.: CO₂ and water vapour fluxes for 2 years
657 above Euroflux forest site, *Agric. For. Meteorol.*, 108(3), 183–197, doi:10.1016/s0168-
658 1923(01)00240-4, 2001.

659

660 Bonan, G. B., Lawrence, P. J., Oleson, K. W., Levis, S., Jung, M., Reichstein, M., Lawrence, D.
661 M. and Swenson, S. C.: Improving canopy processes in the Community Land Model version 4
662 (CLM4) using global flux fields empirically inferred from FLUXNET data, *J. Geophys. Res.*,
663 116(G2), G02014, doi:10.1029/2010JG001593, 2011.

664

665 Bowling, D. R., Bethers-Marchetti, S., Lunch, C. K., Grote, E. E. and Belnap, J.: Carbon, water,
666 and energy fluxes in a semiarid cold desert grassland during and following multiyear drought, *J.*
667 *Geophys. Res.*, 115(G4), G04026, doi:10.1029/2010jg001322, 2010.

668

669 Bükér, P., Feng, Z., Uddling, J., Briolat, A., Alonso, R., Braun, S., Elvira, S., Gerosa, G.,
670 Karlsson, P. E., Le Thiec, D., Marzuoli, R., Mills, G., Oksanen, E., Wieser, G., Wilkinson, M.
671 and Emberson, L. D.: New flux based dose-response relationships for ozone for European forest
672 tree species, *Environ. Pollut.*, 206, 163–174, doi:10.1016/j.envpol.2015.06.033, 2015.

673

674 Carrara, A., Janssens, I. A., Yuste, J. C. and Ceulemans, R.: Seasonal changes in photosynthesis,
675 respiration and NEE of a mixed temperate forest, *Agric. For. Meteorol.*, 126(1–2), 15–31,
676 doi:10.1016/j.agrformet.2004.05.002, 2004.

677

678 Chiesi, M., Maselli, F., Bindi, M., Fibbi, L., Cherubini, P., Arlotta, E., Tirone, G., Matteucci, G.
679 and Seufert, G.: Modelling carbon budget of Mediterranean forests using ground and remote
680 sensing measurements, *Agric. For. Meteorol.*, 135(1–4), 22–34,
681 doi:10.1016/j.agrformet.2005.09.011, 2005.

682

683 Cieslik, S. A.: Ozone uptake by various surface types: A comparison between dose and exposure,
684 *Atmos. Environ.*, 38(15), 2409–2420, doi:10.1016/j.atmosenv.2003.10.063, 2004.

685

686 Claverie, M., Vermote, E. F., Weiss, M., Baret, F., Hagolle, O. and Demarez, V.: Validation of
687 coarse spatial resolution LAI and FAPAR time series over cropland in southwest France, *Remote*
688 *Sens. Environ.*, 139, 216–230, doi:10.1016/j.rse.2013.07.027, 2013.

689

690 Claverie, M., Matthews, J. L., Vermote, E. F. and Justice, C. O.: A 30 + Year AVHRR LAI and
691 FAPAR Climate Data Record : Algorithm Description and Validation, *Remote Sens.*, 8(3), 1–12,
692 doi:10.3390/rs8030263, 2016.

693

694 Clifton, O. E., Fiore, A. M., Munger, J. W., Malyshev, S., Horowitz, L. W., Shevliakova, E.,

695 Paulot, F., Murray, L. T. and Griffin, K. L.: Interannual variability in ozone removal by a
696 temperate deciduous forest, *Geophys. Res. Lett.*, 44(1), 542–552, doi:10.1002/2016GL070923,
697 2017.

698

699 Cook, B. D., Davis, K. J., Wang, W., Desai, A., Berger, B. W., Teclaw, R. M., Martin, J. G.,
700 Bolstad, P. V, Bakwin, P. S., Yi, C. and Heilman, W.: Carbon exchange and venting anomalies
701 in an upland deciduous forest in northern Wisconsin, USA, *Agric. For. Meteorol.*, 126(3–4),
702 271–295, doi:10.1016/j.agrformet.2004.06.008, 2004.

703

704 Delpierre, N., Berveiller, D., Granda, E. and Dufrêne, E.: Wood phenology, not carbon input,
705 controls the interannual variability of wood growth in a temperate oak forest, *New Phytol.*,
706 210(2), 459–470, doi:10.1111/nph.13771, 2015.

707

708 Desai, A. R., Bolstad, P. V, Cook, B. D., Davis, K. J. and Carey, E. V: Comparing net ecosystem
709 exchange of carbon dioxide between an old-growth and mature forest in the upper Midwest,
710 USA, *Agric. For. Meteorol.*, 128(1–2), 33–55, doi:10.1016/j.agrformet.2004.09.005, 2005.

711

712 Desai, A. R., Xu, K., Tian, H., Weishampel, P., Thom, J., Baumann, D., Andrews, A. E., Cook,
713 B. D., King, J. Y. and Kolka, R.: Landscape-level terrestrial methane flux observed from a very
714 tall tower, *Agric. For. Meteorol.*, 201, 61–75, doi:10.1016/j.agrformet.2014.10.017, 2015.

715

716 Dietiker, D., Buchmann, N. and Eugster, W.: Testing the ability of the DNDC model to predict
717 CO₂ and water vapour fluxes of a Swiss cropland site, *Agric. Ecosyst. Environ.*, 139(3), 396–
718 401, doi:10.1016/j.agee.2010.09.002, 2010.

719

720 Van Dingenen, R., Dentener, F. J., Raes, F., Krol, M. C., Emberson, L. and Cofala, J.: The global
721 impact of ozone on agricultural crop yields under current and future air quality legislation,
722 *Atmos. Environ.*, 43(3), 604–618, doi:10.1016/j.atmosenv.2008.10.033, 2009.

723

724 Dolman, A. J., Moors, E. J. and Elbers, J. A.: The carbon uptake of a mid latitude pine forest
725 growing on sandy soil, *Agric. For. Meteorol.*, 111(3), 157–170, doi:10.1016/S0168-
726 1923(02)00024-2, 2002.

727

728 Dragoni, D., Schmid, H. P., Wayson, C. A., Potter, H., Grimmond, C. S. B. and Randolph, J. C.:
729 Evidence of increased net ecosystem productivity associated with a longer vegetated season in a
730 deciduous forest in south-central Indiana, USA, *Glob. Chang. Biol.*, 17(2), 886–897,
731 doi:10.1111/j.1365-2486.2010.02281.x, 2011.

732

733 Drake, P. L., Froend, R. H. and Franks, P. J.: Smaller , faster stomata : scaling of stomatal size ,
734 rate of response , and stomatal conductance, *Exp. Bot.*, 64(2), 495–505, doi:10.1093/jxb/ers347,
735 2013.

736

737 Dušek, J., Čížková, H., Stellner, S., Czerný, R. and Květ, J.: Fluctuating water table affects gross
738 ecosystem production and gross radiation use efficiency in a sedge-grass marsh, *Hydrobiologia*,
739 692(1), 57–66, doi:10.1007/s10750-012-0998-z, 2012.

740

741 El-Madany, T., Niklasch, K. and Klemm, O.: Stomatal and non-stomatal turbulent deposition
742 flux of ozone to a managed peatland, *Atmosphere (Basel)*, 8(9), 175,
743 doi:10.3390/atmos8090175, 2017.
744

745 Etzold, S., Ruehr, N. K., Zweifel, R., Dobbertin, M., Zingg, A., Pluess, P., Häsler, R., Eugster,
746 W. and Buchmann, N.: The carbon balance of two contrasting mountain forest ecosystems in
747 Switzerland: Similar annual trends, but seasonal differences, *Ecosystems*, 14(8), 1289–1309,
748 doi:10.1007/s10021-011-9481-3, 2011.
749

750 Fares, S., McKay, M., Holzinger, R. and Goldstein, A. H.: Ozone fluxes in a *Pinus ponderosa*
751 ecosystem are dominated by non-stomatal processes: Evidence from long-term continuous
752 measurements, *Agric. For. Meteorol.*, 150(3), 420–431, doi:10.1016/j.agrformet.2010.01.007,
753 2010.
754

755 Fares, S., Savi, F., Muller, J., Matteucci, G. and Paoletti, E.: Simultaneous measurements of
756 above and below canopy ozone fluxes help partitioning ozone deposition between its various
757 sinks in a Mediterranean Oak Forest, *Agric. For. Meteorol.*, 198–199, 181–191,
758 doi:10.1016/j.agrformet.2014.08.014, 2014.
759

760 Ferréa, C., Zenone, T., Comolli, R. and Seufert, G.: Estimating heterotrophic and autotrophic soil
761 respiration in a semi-natural forest of Lombardy, Italy, *Pedobiologia (Jena)*, 55(6), 285–294,
762 doi:10.1016/j.pedobi.2012.05.001, 2012.
763

764 Finkelstein, P. L., Ellestad, T. G., Clarke, J. F., Meyers, T. P., Schwede, D. B., Hebert, E. O. and
765 Neal, J. A.: Ozone and sulfur dioxide dry deposition to forests: Observations and model
766 evaluation, *J. Geophys. Res. Atmos.*, 105(D12), 15365–15377, doi:10.1029/2000JD900185,
767 2000.
768

769 Fischer, M. L., Billesbach, D. P., Berry, J. A., Riley, W. J. and Torn, M. S.: Spatiotemporal
770 variations in growing season exchanges of CO₂, H₂O, and sensible heat in agricultural fields of
771 the Southern Great Plains, *Earth Interact.*, 11(17), 1–21, doi:10.1175/ei231.1, 2007.
772

773 Foken, T.: *Micrometeorology*, 2nd edition, Springer, doi:10.1007/978-3-642-25440-6, 2017.
774

775 Frank, J. M., Massman, W. J., Ewers, B. E., Huckaby, L. S. and Negrón, J. F.: Ecosystem
776 CO₂/H₂O fluxes are explained by hydraulically limited gas exchange during tree mortality from
777 spruce bark beetles, *J. Geophys. Res. Biogeosciences*, 119(6), 1195–1215,
778 doi:10.1002/2013jg002597, 2014.
779

780 Fuhrer, J.: Introduction to the special issue on ozone risk analysis for vegetation in Europe.,
781 *Environ. Pollut.*, 109(3), 359–60 [online] Available from:
782 <http://www.ncbi.nlm.nih.gov/pubmed/15092869>, 2000.
783

784 Fuhrer, J., Skärby, L. and Ashmore, M. R.: Critical levels for ozone effects on vegetation in
785 Europe, *Environ. Pollut.*, 97(1–2), 91–106, doi:10.1016/S0269-7491(97)00067-5, 1997.
786

787 Galvagno, M., Wohlfahrt, G., Cremonese, E., Rossini, M., Colombo, R., Filippa, G., Julitta, T.,
788 Manca, G., Siniscalco, C., di Cella, U. M. and Migliavacca, M.: Phenology and carbon dioxide
789 source/sink strength of a subalpine grassland in response to an exceptionally short snow season,
790 *Environ. Res. Lett.*, 8(2), 25008, doi:10.1088/1748-9326/8/2/025008, 2013.

791
792 Garbulsky, M. F., Penuelas, J., Papale, D. and Filella, I.: Remote estimation of carbon dioxide
793 uptake by a Mediterranean forest, *Glob. Chang. Biol.*, 14(12), 2860–2867, doi:10.1111/j.1365-
794 2486.2008.01684.x, 2008.

795
796 Gelaro, R., McCarty, W., Suárez, M. J., Todling, R., Molod, A., Takacs, L., Randles, C. A.,
797 Darmenov, A., Bosilovich, M. G., Reichle, R., Wargan, K., Coy, L., Cullather, R., Draper, C.,
798 Akella, S., Buchard, V., Conaty, A., da Silva, A. M., Gu, W., Kim, G. K., Koster, R., Lucchesi,
799 R., Merkova, D., Nielsen, J. E., Partyka, G., Pawson, S., Putman, W., Rienecker, M., Schubert,
800 S. D., Sienkiewicz, M. and Zhao, B.: The modern-era retrospective analysis for research and
801 applications, version 2 (MERRA-2), *J. Clim.*, 30(14), 5419–5454, doi:10.1175/JCLI-D-16-
802 0758.1, 2017.

803
804 Gentine, P., Chhang, A., Rigden, A. and Salvucci, G.: Evaporation estimates using weather
805 station data and boundary layer theory, *Geophys. Res. Lett.*, 43(11), 661–670,
806 doi:10.1002/2016GL070819, 2016.

807
808 Gerosa, G., Marzuoli, R., Cieslik, S. and Ballarin-Denti, A.: Stomatal ozone fluxes over a barley
809 field in Italy. “Effective exposure” as a possible link between exposure- and flux-based
810 approaches, *Atmos. Environ.*, 38(15), 2421–2432, doi:10.1016/j.atmosenv.2003.12.040, 2004.

811
812 Gerosa, G., Vitale, M., Finco, A., Manes, F., Denti, A. B. and Cieslik, S.: Ozone uptake by an
813 evergreen Mediterranean Forest (*Quercus ilex*) in Italy. Part I: Micrometeorological flux
814 measurements and flux partitioning, *Atmos. Environ.*, 39(18), 3255–3266,
815 doi:10.1016/j.atmosenv.2005.01.056, 2005.

816
817 Gerosa, G., Derghi, F. and Cieslik, S.: Comparison of different algorithms for stomatal ozone
818 flux determination from micrometeorological measurements, *Water. Air. Soil Pollut.*, 179(1–4),
819 309–321, doi:10.1007/s11270-006-9234-7, 2007.

820
821 Goldstein, A. H., Hultman, N. E., Fracheboud, J. M., Bauer, M. R., Panek, J. a., Xu, M., Qi, Y.,
822 Guenther, A. B. and Baugh, W.: Effects of climate variability on the carbon dioxide, water, and
823 sensible heat fluxes above a ponderosa pine plantation in the Sierra Nevada (CA), *Agric. For.*
824 *Meteorol.*, 101(2–3), 113–129, doi:10.1016/S0168-1923(99)00168-9, 2000.

825
826 Gough, C. M., Hardiman, B. S., Nave, L. E., Bohrer, G., Maurer, K. D., Vogel, C. S.,
827 Nadelhoffer, K. J. and Curtis, P. S.: Sustained carbon uptake and storage following moderate
828 disturbance in a Great Lakes forest, *Ecol. Appl.*, 23(5), 1202–1215, doi:10.1890/12-1554.1,
829 2013.

830
831 Grünwald, T. and Bernhofer, C.: A decade of carbon, water and energy flux measurements of an
832 old spruce forest at the Anchor Station Tharandt, *Tellus Ser. B-Chemical Phys. Meteorol.*, 59(3),

833 387–396, doi:10.3402/tellusb.v59i3.17000, 2007.
834
835 Guidi, L., Nali, C., Lorenzini, G., Filippi, F. and Soldatini, G. F.: Effect of chronic ozone
836 fumigation on the photosynthetic process of poplar clones showing different sensitivity, *Environ.*
837 *Pollut.*, 113(3), 245–254, doi:10.1016/S0269-7491(00)00194-9, 2001.
838
839 Hardacre, C., Wild, O. and Emberson, L.: An evaluation of ozone dry deposition in global scale
840 chemistry climate models, *Atmos. Chem. Phys.*, 15(11), 6419–6436, doi:10.5194/acp-15-6419-
841 2015, 2015.
842
843 Hatala, J. A., Detto, M., Sonnentag, O., Deverel, S. J., Verfaillie, J. and Baldocchi, D. D.:
844 Greenhouse gas (CO₂, CH₄, H₂O) fluxes from drained and flooded agricultural peatlands in the
845 Sacramento-San Joaquin Delta, *Agric. Ecosyst. Environ.*, 150, 1–18,
846 doi:10.1016/j.agee.2012.01.009, 2012.
847
848 Holtslag, a. a. M. and De Bruin, H. a. R.: Applied modeling of the nighttime surface energy
849 balance over land, *J. Appl. Meteorol.*, 27(6), 689–704, doi:10.1175/1520-
850 0450(1988)027<0689:AMOTNS>2.0.CO;2, 1988.
851
852 Hommeltenberg, J., Schmid, H. P., Drösler, M. and Werle, P.: Can a bog drained for forestry be
853 a stronger carbon sink than a natural bog forest?, *Biogeosciences*, 11(13), 3477–3493,
854 doi:10.5194/bg-11-3477-2014, 2014.
855
856 Hoshika, Y., Katata, G., Deushi, M., Watanabe, M., Koike, T. and Paoletti, E.: Ozone-induced
857 stomatal sluggishness changes carbon and water balance of temperate deciduous forests, *Sci.*
858 *Rep.*, 5, 9871, doi:10.1038/srep09871, 2015.
859
860 Imer, D., Merbold, L., Eugster, W. and Buchmann, N.: Temporal and spatial variations of soil
861 CO₂, CH₄ and N₂O fluxes at three differently managed grasslands, *Biogeosciences*, 10(9),
862 5931–5945, doi:10.5194/bg-10-5931-2013, 2013.
863
864 Irvine, J., Law, B. E. and Hibbard, K. A.: Postfire carbon pools and fluxes in semiarid ponderosa
865 pine in Central Oregon, *Glob. Chang. Biol.*, 13(8), 1748–1760, doi:10.1111/j.1365-
866 2486.2007.01368.x, 2007.
867
868 Irvine, J., Law, B. E., Martin, J. G. and Vickers, D.: Interannual variation in soil CO₂ efflux and
869 the response of root respiration to climate and canopy gas exchange in mature ponderosa pine,
870 *Glob. Chang. Biol.*, 14(12), 2848–2859, doi:10.1111/j.1365-2486.2008.01682.x, 2008.
871
872 Jacobs, C. M. J., Jacobs, A. F. G., Bosveld, F. C., Hendriks, D. M. D., Hensen, A., Kroon, P. S.,
873 Moors, E. J., Nol, L., Schrier-Uijl, A. and Veenendaal, E. M.: Variability of annual CO₂
874 exchange from Dutch grasslands, *Biogeosciences*, 4(5), 803–816, doi:10.5194/bg-4-803-2007,
875 2007.
876
877 Jacobson, M. Z.: *Fundamentals of atmospheric modeling* second edition, Cambridge University
878 Press., 2005.

879
880 Karlsson, P. E., Uddling, J., Braun, S., Broadmeadow, M., Elvira, S., Gimeno, B. S., Le Thiec,
881 D., Oksanen, E., Vandermeiren, K., Wilkinson, M. and Emberson, L.: New critical levels for
882 ozone effects on young trees based on AOT40 and simulated cumulative leaf uptake of ozone,
883 *Atmos. Environ.*, 38(15), 2283–2294, doi:10.1016/j.atmosenv.2004.01.027, 2004.
884
885 Kavassalis, S. C. and Murphy, J. G.: Understanding ozone-meteorology correlations: A role for
886 dry deposition, *Geophys. Res. Lett.*, 44(6), 2922–2931, doi:10.1002/2016GL071791, 2017.
887
888 Keronen, P., Reissell, A., Rannik, Ü., Pohja, T., Siivola, E., Hiltunen, V., Hari, P., Kulmala, M.
889 and Vesala, T.: Ozone flux measurements over a Scots pine forest using eddy covariance
890 method: Performance evaluation and comparison with flux-profile method, *Boreal Environ. Res.*,
891 8(4), 425–443 [online] Available from: <http://www.scopus.com/inward/record.url?eid=2-s2.0-0347884158&partnerID=40&md5=4ad114fb52c557d36cc8a0ec1ab8bb7e>, 2003.
892
893
894 Knauer, J., Zaehle, S., Medlyn, B. E., Reichstein, M., Werner, C., Keitel, C., Williams, C. A.,
895 Migliavacca, M., Kauwe, M. G. De, Kolari, P., Limousin, J.-M. and Linderson, M.-L.: Towards
896 physiologically meaningful water-use efficiency estimates from eddy covariance data,
897 *Biogeosciences*, 15(8), 694–710, doi:10.1111/gcb.13893, 2017.
898
899 Knohl, A., Schulze, E.-D., Kolle, O. and Buchmann, N.: Large carbon uptake by an unmanaged
900 250-year-old deciduous forest in Central Germany, *Agric. For. Meteorol.*, 118(3–4), 151–167,
901 doi:10.1016/s0168-1923(03)00115-1, 2003.
902
903 Knox, S. H., Matthes, J. H., Sturtevant, C., Oikawa, P. Y., Verfaillie, J. and Baldocchi, D.:
904 Biophysical controls on interannual variability in ecosystem-scale CO₂ and CH₄ exchange in a
905 California rice paddy, *J. Geophys. Res. Biogeosciences*, 121(3), 978–1001,
906 doi:10.1002/2015jg003247, 2016.
907
908 Kurbatova, J., Li, C., Varlagin, A., Xiao, X. and Vygodskaya, N.: Modeling carbon dynamics in
909 two adjacent spruce forests with different soil conditions in Russia, *Biogeosciences*, 5(4), 969–
910 980, doi:10.5194/bg-5-969-2008, 2008.
911
912 Kurpius, M. R. and Goldstein, A. H.: Gas-phase chemistry dominates O₃ loss to a forest,
913 implying a source of aerosols and hydroxyl radicals to the atmosphere, *Geophys. Res. Lett.*,
914 30(7), 2–5, doi:10.1029/2002GL016785, 2003.
915
916 Lamaud, E., Loubet, B., Irvine, M., Stella, P., Personne, E. and Cellier, P.: Partitioning of ozone
917 deposition over a developed maize crop between stomatal and non-stomatal uptakes, using eddy-
918 covariance flux measurements and modelling, *Agric. For. Meteorol.*, 149(9), 1385–1396,
919 doi:10.1016/j.agrformet.2009.03.017, 2009.
920
921 Launiainen, S., Rinne, J., Pumpanen, J., Kulmala, L., Kolari, P., Keronen, P., Siivola, E., Pohja,
922 T., Hari, P. and Vesala, T.: Eddy covariance measurements of CO₂ and sensible and latent heat
923 fluxes during a full year in a boreal pine forest trunk-space, *Boreal Environ. Res.*, 10(6), 569–
924 588, 2005.

925
926 Lefohn, A. S. and Runeckles, V. C.: Establishing standards to protect vegetation-ozone
927 exposure/dose considerations, *Atmos. Environ.*, 21(3), 561–568, doi:10.1016/0004-
928 6981(87)90038-2, 1987.
929
930 Lin, C., Gentine, P., Huang, Y., Guan, K., Kimm, H. and Zhou, S.: Diel ecosystem conductance
931 response to vapor pressure deficit is suboptimal and independent of soil moisture, *Agric. For.*
932 *Meteorol.*, 250–251(2017), 24–34, doi:10.1016/j.agrformet.2017.12.078, 2018.
933
934 Lindauer, M., Schmid, H. P., Grote, R., Mauder, M., Steinbrecher, R. and Wolpert, B.: Net
935 ecosystem exchange over a non-cleared wind-throw-disturbed upland spruce forest—
936 Measurements and simulations, *Agric. For. Meteorol.*, 197, 219–234,
937 doi:10.1016/j.agrformet.2014.07.005, 2014.
938
939 Lohila, A.: Annual CO₂ exchange of a peat field growing spring barley or perennial forage grass,
940 *J. Geophys. Res.*, 109, D18116, doi:10.1029/2004jd004715, 2004.
941
942 Lombardozi, D., Sparks, J. P., Bonan, G. and Levis, S.: Ozone exposure causes a decoupling of
943 conductance and photosynthesis: Implications for the Ball-Berry stomatal conductance model,
944 *Oecologia*, 169(3), 651–659, doi:10.1007/s00442-011-2242-3, 2012.
945
946 Lombardozi, D., Sparks, J. P. and Bonan, G.: Integrating O₃ influences on terrestrial processes:
947 photosynthetic and stomatal response data available for regional and global modeling,
948 *Biogeosciences*, 10, 6815–6831, doi:10.5194/bg-10-6815-2013, 2013.
949
950 Lombardozi, D., Levis, S., Bonan, G., Hess, P. G. and Sparks, J. P.: The influence of chronic
951 ozone exposure on global carbon and water cycles, *J. Clim.*, 28(1), 292–305, doi:10.1175/JCLI-
952 D-14-00223.1, 2015.
953
954 Loubet, B., Laville, P., Lehuger, S., Larmanou, E., Fléchar, C., Mascher, N., Genermont, S.,
955 Roche, R., Ferrara, R. M., Stella, P., Personne, E., Durand, B., Decuq, C., Flura, D., Masson, S.,
956 Fanucci, O., Rampon, J.-N., Siemens, J., Kindler, R., Gabrielle, B., Schrupf, M. and Cellier, P.:
957 Carbon, nitrogen and Greenhouse gases budgets over a four years crop rotation in northern
958 France, *Plant Soil*, 343(1–2), 109–137, doi:10.1007/s11104-011-0751-9, 2011.
959
960 Ma, S., Baldocchi, D. D., Xu, L. and Hehn, T.: Inter-annual variability in carbon dioxide
961 exchange of an oak/grass savanna and open grassland in California, *Agric. For. Meteorol.*,
962 147(3–4), 157–171, doi:10.1016/j.agrformet.2007.07.008, 2007.
963
964 Mammarella, I., Kolari, P., Rinne, J., Keronen, P., Pumpanen, J. and Vesala, T.: Determining the
965 contribution of vertical advection to the net ecosystem exchange at Hyytiälä forest, Finland,
966 *Tellus, Ser. B Chem. Phys. Meteorol.*, 59(5), 900–909, doi:10.1111/j.1600-0889.2007.00306.x,
967 2007.
968
969 Marcolla, B., Pitacco, A. and Cescatti, A.: Canopy architecture and turbulence structure in a
970 coniferous forest, *Boundary-Layer Meteorol.*, 108(1), 39–59, doi:10.1023/a:1023027709805,

971 2003.
972
973 Marcolla, B., Cescatti, A., Manca, G., Zorer, R., Cavagna, M., Fiora, A., Gianelle, D.,
974 Rodeghiero, M., Sottocornola, M. and Zampedri, R.: Climatic controls and ecosystem responses
975 drive the inter-annual variability of the net ecosystem exchange of an alpine meadow, *Agric. For.*
976 *Meteorol.*, 151(9), 1233–1243, doi:10.1016/j.agrformet.2011.04.015, 2011.
977
978 Marrero, T. R. and Mason, E. A.: Gaseous Diffusion Coefficients, *J. Phys. Chem. Ref. Data*,
979 1(1), 3–118, doi:10.1063/1.3253094, 1972.
980
981 Matthes, J. H., Sturtevant, C., Verfaillie, J., Knox, S. and Baldocchi, D.: Parsing the variability in
982 CH₄ flux at a spatially heterogeneous wetland: Integrating multiple eddy covariance towers with
983 high-resolution flux footprint analysis, *J. Geophys. Res. Biogeosciences*, 119(7), 1322–1339,
984 doi:10.1002/2014jg002642, 2014.
985
986 Matyssek, R., Bahnweg, G., Ceulemans, R., Fabian, P., Grill, D., Hanke, D. E., Kraigher, H.,
987 Oßwald, W., Rennenberg, H., Sandermann, H., Tausz, M. and Wieser, G.: Synopsis of the
988 CASIROZ case study: Carbon sink strength of *Fagus sylvatica* L. in a changing environment -
989 Experimental risk assessment of mitigation by chronic ozone impact, *Plant Biol.*, 9(2), 163–180,
990 doi:10.1055/s-2007-964883, 2007.
991
992 Matyssek, R., Karnosky, D. F., Wieser, G., Percy, K., Oksanen, E., Grams, T. E. E., Kubiske,
993 M., Hanke, D. and Pretzsch, H.: Advances in understanding ozone impact on forest trees:
994 Messages from novel phytotron and free-air fumigation studies, *Environ. Pollut.*, 158(6), 1990–
995 2006, doi:10.1016/j.envpol.2009.11.033, 2010.
996
997 Mauder, M., Cuntz, M., Drüe, C., Graf, A., Rebmann, C., Schmid, H. P., Schmidt, M. and
998 Steinbrecher, R.: A strategy for quality and uncertainty assessment of long-term eddy-covariance
999 measurements, *Agric. For. Meteorol.*, 169, 122–135, doi:10.1016/j.agrformet.2012.09.006, 2013.
1000
1001 McKinney, W.: Data Structures for Statistical Computing in Python, in *Proceedings of the 9th*
1002 *Python in Science Conference*, edited by S. Van Der Walt, pp. 51–56., 2010.
1003
1004 Medlyn, B. E., Duursma, R. A., Eamus, D., Ellsworth, D. S., Prentice, I. C., Barton, C. V. M.,
1005 Crous, K. Y., De Angelis, P., Freeman, M. and Wingate, L.: Reconciling the optimal and
1006 empirical approaches to modelling stomatal conductance, *Glob. Chang. Biol.*, 17(6), 2134–2144,
1007 doi:10.1111/j.1365-2486.2010.02375.x, 2011.
1008
1009 Merbold, L., Eugster, W., Stieger, J., Zahniser, M., Nelson, D. and Buchmann, N.: Greenhouse
1010 gas budget (CO₂, CH₄, and N₂O) of intensively managed grassland following restoration, *Glob.*
1011 *Chang. Biol.*, 20(6), 1913–1928, doi:10.1111/gcb.12518, 2014.
1012
1013 Migliavacca, M., Meroni, M., Busetto, L., Colombo, R., Zenone, T., Matteucci, G., Manca, G.
1014 and Seufert, G.: Modeling gross primary production of agro-forestry ecosystems by assimilation
1015 of satellite-derived information in a process-based model, *Sensors*, 9(2), 922–942,
1016 doi:10.3390/s90200922, 2009.

1017
1018 Mills, G., Hayes, F., Simpson, D., Emberson, L., Norris, D., Harmens, H. and Büker, P.:
1019 Evidence of widespread effects of ozone on crops and (semi-)natural vegetation in Europe
1020 (1990-2006) in relation to AOT40- and flux-based risk maps, *Glob. Chang. Biol.*, 17(1), 592–
1021 613, doi:10.1111/j.1365-2486.2010.02217.x, 2011.
1022
1023 Monson, R. K., Turnipseed, A. A., Sparks, J. P., Harley, P. C., Scott-Denton, L. E., Sparks, K.
1024 and Huxman, T. E.: Carbon sequestration in a high-elevation, subalpine forest, *Glob. Chang.*
1025 *Biol.*, 8(5), 459–478, doi:10.1046/j.1365-2486.2002.00480.x, 2002.
1026
1027 Montagnani, L., Manca, G., Canepa, E., Georgieva, E., Acosta, M., Feigenwinter, C., Janous, D.,
1028 Kerschbaumer, G., Lindroth, A., Minach, L., Minerbi, S., Mölder, M., Pavelka, M., Seufert, G.,
1029 Zeri, M. and Ziegler, W.: A new mass conservation approach to the study of CO₂ advection in
1030 an alpine forest, *J. Geophys. Res.*, 114(D7), D07306, doi:10.1029/2008jd010650, 2009.
1031
1032 Monteith, J. L.: Evaporation and surface temperature, *Quaterly J. R. Meteorol. Soc.*, 107(451),
1033 1–27, 1981.
1034
1035 Moore, K. E., Fitzjarrald, D. R., Sakai, R. K., Goulden, M. L., Munger, J. W. and Wofsy, S. C.:
1036 Seasonal variation in radiative and turbulent exchange at a deciduous forest in central
1037 Massachusetts, *J. Appl. Meteorology*, 35, 122–134, doi:10.1175/1520-
1038 0450(1996)035<0122:SVIRAT>2.0.CO;2, 1996.
1039
1040 Morin, T. H., Bohrer, G., d. M. Frasson, R. P., Naor-Azreli, L., Mesi, S., Stefanik, K. C. and
1041 Schäfer, K. V. R.: Environmental drivers of methane fluxes from an urban temperate wetland
1042 park, *J. Geophys. Res. Biogeosciences*, 119(11), 2188–2208, doi:10.1002/2014jg002750, 2014.
1043 Moureaux, C., Debacq, A., Bodson, B., Heinesch, B. and Aubinet, M.: Annual net ecosystem
1044 carbon exchange by a sugar beet crop, *Agric. For. Meteorol.*, 139(1–2), 25–39,
1045 doi:10.1016/j.agrformet.2006.05.009, 2006.
1046
1047 Munger, J. W., Wofsy, S. C., Bakwin, P. S., Fan, S., Goulden, M. L., Daube, B. C., Goldstein, A.
1048 H., Moore, K. E. and Fitzjarrald, D. R.: Atmospheric deposition of reactive nitrogen oxides and
1049 ozaone in a temperate deciduos forest and a subartic woodland 1. Measurements and
1050 mechanisms, *J. Geophys. Res.*, 101, 12639–12657, 1996.
1051
1052 Musselman, R. C., Lefohn, A. S., Massman, W. J. and Heath, R. L.: A critical review and
1053 analysis of the use of exposure- and flux-based ozone indices for predicting vegetation effects,
1054 *Atmos. Environ.*, 40(10), 1869–1888, doi:10.1016/j.atmosenv.2005.10.064, 2006.
1055
1056 Noormets, A., Chen, J. and Crow, T. R.: Age-Dependent Changes in Ecosystem Carbon Fluxes
1057 in Managed Forests in Northern Wisconsin, USA, *Ecosystems*, 10(2), 187–203,
1058 doi:10.1007/s10021-007-9018-y, 2007.
1059
1060 Novick, K. A., Ficklin, D. L., Stoy, P. C., Williams, C. A., Bohrer, G., Oishi, A. C., Papuga, S.
1061 A., Blanken, P. D., Noormets, A., Sulman, B. N., Scott, R. L., Wang, L. and Phillips, R. P.: The

1062 increasing importance of atmospheric demand for ecosystem water and carbon fluxes, *Nat. Clim.*
1063 *Chang.*, 6(11), 1023–1027, doi:10.1038/nclimate3114, 2016.

1064

1065 Oikawa, P. Y., Jenerette, G. D., Knox, S. H., Sturtevant, C., Verfaillie, J., Dronova, I.,
1066 Poindexter, C. M., Eichelmann, E. and Baldocchi, D. D.: Evaluation of a hierarchy of models
1067 reveals importance of substrate limitation for predicting carbon dioxide and methane exchange in
1068 restored wetlands, *J. Geophys. Res. Biogeosciences*, 122(1), 145–167,
1069 doi:10.1002/2016jg003438, 2017.

1070

1071 Paoletti, E. and Manning, W. J.: Toward a biologically significant and usable standard for ozone
1072 that will also protect plants, *Environ. Pollut.*, 150(1), 85–95, doi:10.1016/j.envpol.2007.06.037,
1073 2007.

1074

1075 Papale, D., Migliavacca, M., Cremonese, E., Cescatti, A., Alberti, G., Balzarolo, M., Marchesini,
1076 L. B., Canfora, E., Casa, R., Duce, P., Facini, O., Galvagno, M., Genesio, L., Gianelle, D.,
1077 Magliulo, V., Matteucci, G., Montagnani, L., Petrella, F., Pitacco, A., Seufert, G., Spano, D.,
1078 Stefani, P., Vaccari, F. P. and Valentini, R.: Carbon, water and anergy fluxes of terrestrial
1079 ecosystems in Italy, in *The Greenhouse Gas Balance of Italy*, pp. 11–45, Springer, Berlin
1080 Heidelberg., 2015.

1081

1082 Pastorello, G., Agarwal, D., Papale, D., Samak, T., Trotta, C., Ribeca, A., Poindexter, C.,
1083 Faybishenko, B., Gunter, D., Hollowgrass, R. and Canfora, E.: Observational data patterns for
1084 time series data quality assessment, 2014 IEEE 10th Int. Conf. e-Science, 271–278,
1085 doi:10.1109/eScience.2014.45, 2014.

1086

1087 Pastorello, G., Papale, D., Chu, H., Trotta, C., Agarwal, D., Canfora, E., Baldocchi, D. and Torn,
1088 M.: A new data set to keep a sharper eye on land-air exchanges, *Eos (Washington. DC)*., 98,
1089 doi:10.1029/2017EO071597, 2017.

1090

1091 Plake, D., Stella, P., Moravek, A., Mayer, J. C., Ammann, C., Held, A. and Trebs, I.:
1092 Comparison of ozone deposition measured with the dynamic chamber and the eddy covariance
1093 method, *Agric. For. Meteorol.*, 206, 97–112, doi:10.1016/j.agrformet.2015.02.014, 2015.

1094

1095 Pleijel, H., Danielsson, H., Ojanperä, K., De Temmerman, L., Högy, P., Badiani, M. and
1096 Karlsson, P. E.: Relationships between ozone exposure and yield loss in European wheat and
1097 potato - A comparison of concentration- and flux-based exposure indices, *Atmos. Environ.*,
1098 38(15), 2259–2269, doi:10.1016/j.atmosenv.2003.09.076, 2004.

1099

1100 Pleijel, H., Danielsson, H., Simpson, D. and Mills, G.: Have ozone effects on carbon
1101 sequestration been overestimated? A new biomass response function for wheat, *Biogeosciences*,
1102 11(16), 4521–4528, doi:10.5194/bg-11-4521-2014, 2014.

1103

1104 Pilegaard, K., Ibrom, A., Courtney, M. S., Hummelshøj, P. and Jensen, N. O.: Increasing net
1105 CO₂ uptake by a Danish beech forest during the period from 1996 to 2009, *Agric. For.*
1106 *Meteorol.*, 151(7), 934–946, doi:10.1016/j.agrformet.2011.02.013, 2011.

1107

1108 Post, H., Franssen, H. J. H., Graf, A., Schmidt, M. and Vereecken, H.: Uncertainty analysis of
1109 eddy covariance CO₂ flux measurements for different EC tower distances using an extended
1110 two-tower approach, *Biogeosciences*, 12(4), 1205–1221, doi:10.5194/bg-12-1205-2015, 2015.
1111

1112 Powell, T. L., Bracho, R., Li, J., Dore, S., Hinkle, C. R. and Drake, B. G.: Environmental
1113 controls over net ecosystem carbon exchange of scrub oak in central Florida, *Agric. For.
1114 Meteorol.*, 141(1), 19–34, doi:10.1016/j.agrformet.2006.09.002, 2006.
1115

1116 Prescher, A.-K., Grünwald, T. and Bernhofer, C.: Land use regulates carbon budgets in eastern
1117 Germany: From NEE to NBP, *Agric. For. Meteorol.*, 150(7–8), 1016–1025,
1118 doi:10.1016/j.agrformet.2010.03.008, 2010.
1119

1120 Rambal, S., Joffre, R., Ourcival, J. M., Cavender-Bares, J. and Rocheteau, A.: The growth
1121 respiration component in eddy CO₂ flux from a *Quercus ilex mediterranean* forest, *Glob. Chang.
1122 Biol.*, 10(9), 1460–1469, doi:10.1111/j.1365-2486.2004.00819.x, 2004.
1123

1124 Rannik, Ü., Mammarella, I., Keronen, P. and Vesala, T.: Vertical advection and nocturnal
1125 deposition of ozone over a boreal pine forest, *Atmos. Chem. Phys.*, 9(6), 2089–2095,
1126 doi:10.5194/acp-9-2089-2009, 2009.
1127

1128 Rannik, Ü., Altimir, N., Mammarella, I., Bäck, J., Rinne, J., Ruuskanen, T. M., Hari, P., Vesala,
1129 T. and Kulmala, M.: Ozone deposition into a boreal forest over a decade of observations:
1130 Evaluating deposition partitioning and driving variables, *Atmos. Chem. Phys.*, 12(24), 12165–
1131 12182, doi:10.5194/acp-12-12165-2012, 2012.
1132

1133 Raz-Yaseef, N., Billesbach, D. P., Fischer, M. L., Biraud, S. C., Gunter, S. A., Bradford, J. A.
1134 and Torn, M. S.: Vulnerability of crops and native grasses to summer drying in the U.S. Southern
1135 Great Plains, *Agric. Ecosyst. Environ.*, 213, 209–218, doi:10.1016/j.agee.2015.07.021, 2015.
1136

1137 Reda, I. and Andreas, A.: Solar position algorithm for solar radiation applications, *Sol. Energy*,
1138 76(5), 577–589, doi:10.1016/j.solener.2003.12.003, 2004.
1139

1140 Reich, P. B.: Quantifying plant response to ozone: A unifying theory, *Tree Physiol.*, 3(0), 63–91,
1141 doi:10.1093/treephys/3.1.63, 1987.
1142

1143 Reich, P. B. and Amundson, R. G.: Ambient levels of ozone reduce net photosynthesis in tree
1144 and crop species, *Science (80-.)*, 230(11), 566–570, 1985.
1145

1146 Reich, P. B. and Lassoie, J. P.: Effects of low level O₃ exposure on leaf diffusive conductance
1147 and water-use efficiency in hybrid poplar, *Plant. Cell Environ.*, 7(9), 661–668,
1148 doi:10.1111/1365-3040.ep11571645, 1984.
1149

1150 Reichle, R., Draper, C., Liu, Q., Girotto, M., Mahanama, S., Koster, R. and Lannoy, G.:
1151 Assessment of MERRA-2 Land Surface Hydrology Estimates, *Am. Meteorol. Soc. J. Clim.*,
1152 30(8), 2937–2960, doi:10.1175/JCLI-D-16-0720.1, 2017.
1153

1154 Reichstein, M., Falge, E., Baldocchi, D., Papale, D., Aubinet, M., Berbigier, P., Bernhofer, C.,
 1155 Buchmann, N., Gilmanov, T., Granier, A., Grünwald, T., Havránková, K., Ilvesniemi, H.,
 1156 Janous, D., Knohl, A., Laurila, T., Lohila, A., Loustau, D., Matteucci, G., Meyers, T., Miglietta,
 1157 F., Ourcival, J. M., Pumpanen, J., Rambal, S., Rotenberg, E., Sanz, M., Tenhunen, J., Seufert, G.,
 1158 Vaccari, F., Vesala, T., Yakir, D. and Valentini, R.: On the separation of net ecosystem exchange
 1159 into assimilation and ecosystem respiration: Review and improved algorithm, *Glob. Chang.*
 1160 *Biol.*, 11(9), 1424–1439, doi:10.1111/j.1365-2486.2005.001002.x, 2005.
 1161
 1162 Reverter, B. R., Sánchez-Cañete, E. P., Resco, V., Serrano-Ortiz, P., Oyonarte, C. and Kowalski,
 1163 A. S.: Analyzing the major drivers of NEE in a Mediterranean alpine shrubland, *Biogeosciences*,
 1164 7(9), 2601–2611, doi:10.5194/bg-7-2601-2010, 2010.
 1165
 1166 Rey, A., Pegoraro, E., Tedeschi, V., Parri, I. De, Jarvis, P. G. and Valentini, R.: Annual variation
 1167 in soil respiration and its components in a coppice oak forest in Central Italy, *Glob. Chang. Biol.*,
 1168 8(9), 851–866, doi:10.1046/j.1365-2486.2002.00521.x, 2002.
 1169
 1170 Ruehr, N. K., Martin, J. G. and Law, B. E.: Effects of water availability on carbon and water
 1171 exchange in a young ponderosa pine forest: Above- and belowground responses, *Agric. For.*
 1172 *Meteorol.*, 164, 136–148, doi:10.1016/j.agrformet.2012.05.015, 2012.
 1173
 1174 Sabbatini, S., Arriga, N., Bertolini, T., Castaldi, S., Chiti, T., Consalvo, C., Djomo, S. N., Gioli,
 1175 B., Matteucci, G. and Papale, D.: Greenhouse gas balance of cropland conversion to bioenergy
 1176 poplar short-rotation coppice, *Biogeosciences*, 13(1), 95–113, doi:10.5194/bg-13-95-2016, 2016.
 1177
 1178 Schmidt, M., Reichenau, T. G., Fiener, P. and Schneider, K.: The carbon budget of a winter
 1179 wheat field: An eddy covariance analysis of seasonal and inter-annual variability, *Agric. For.*
 1180 *Meteorol.*, 165, 114–126, doi:10.1016/j.agrformet.2012.05.012, 2012.
 1181
 1182 Schnell, J. L., Holmes, C. D., Jangam, A. and Prather, M. J.: Skill in forecasting extreme ozone
 1183 pollution episodes with a global atmospheric chemistry model, *Atmos. Chem. Phys.*, 14(15),
 1184 7721–7739, doi:10.5194/acp-14-7721-2014, 2014.
 1185
 1186 Schwede, D., Zhang, L., Vet, R. and Lear, G.: An intercomparison of the deposition models used
 1187 in the CASTNET and CAPMoN networks, *Atmos. Environ.*, 45(6), 1337–1346,
 1188 doi:10.1016/j.atmosenv.2010.11.050, 2011.
 1189
 1190 Scott, R. L., Jenerette, G. D., Potts, D. L. and Huxman, T. E.: Effects of seasonal drought on net
 1191 carbon dioxide exchange from a woody-plant-encroached semiarid grassland, *J. Geophys. Res.*,
 1192 114(G4), G04004, doi:10.1029/2008jg000900, 2009.
 1193
 1194 Scott, R. L., Hamerlynck, E. P., Jenerette, G. D., Moran, M. S. and Barron-Gafford, G. A.:
 1195 Carbon dioxide exchange in a semidesert grassland through drought-induced vegetation change,
 1196 *J. Geophys. Res.*, 115(G3), G03026, doi:10.1029/2010jg001348, 2010.
 1197
 1198 Scott, R. L., Biederman, J. A., Hamerlynck, E. P. and Barron-Gafford, G. A.: The carbon balance
 1199 pivot point of southwestern U.S. semiarid ecosystems: Insights from the 21st century drought, *J.*

1200 Geophys. Res. Biogeosciences, 120(12), 2612–2624, doi:10.1002/2015jg003181, 2015.
1201
1202 Scott, R. L. and Biederman, J. A.: Partitioning evapotranspiration using long-term carbon
1203 dioxide and water vapor fluxes, *Geophys. Res. Lett.*, 44(13), 6833–6840,
1204 doi:10.1002/2017GL074324, 2017.
1205
1206 Seabold, S. and Perktold, J.: Statsmodels: econometric and statistical modeling with Python, in
1207 Proceedings of the 9th Python in Science Conference, pp. 57–61. [online] Available from:
1208 <http://conference.scipy.org/proceedings/scipy2010/pdfs/seabold.pdf>⁹<http://conference.scipy.org/proceedings/scipy2010/seabold.html>, 2010.
1209
1210
1211 Sen, P. K.: Estimates of the regression coefficient based on Kendall’s tau, *J. Am. Stat. Assoc.*,
1212 63(324), 1379–1389, doi:10.1080/01621459.1968.10480934, 1968.
1213
1214 Silva, S. J. and Heald, C. L.: Investigating dry deposition of ozone to vegetation, *J. Geophys.*
1215 *Res. Atmos.*, 123, 559–573, doi:10.1002/2017JD027278, 2018.
1216
1217 Sitch, S., Cox, P. M., Collins, W. J. and Huntingford, C.: Indirect radiative forcing of climate
1218 change through ozone effects on the land-carbon sink., *Nature*, 448, 791–794,
1219 doi:10.1038/nature06059, 2007.
1220
1221 Stella, P., Personne, E., Loubet, B., Lamaud, E., Ceschia, E., Béziat, P., Bonnefond, J. M., Irvine,
1222 M., Keravec, P., Mascher, N. and Cellier, P.: Predicting and partitioning ozone fluxes to maize
1223 crops from sowing to harvest: The Surf atm-O₃ model, *Biogeosciences*, 8(10), 2869–2886,
1224 doi:10.5194/bg-8-2869-2011, 2011.
1225
1226 Stella, P., Loubet, B., Lamaud, E., Laville, P. and Cellier, P.: Ozone deposition onto bare soil : A
1227 new parameterization, *Agric. For. Meteorol.*, 151(6), 669–681,
1228 doi:10.1016/j.agrformet.2011.01.015, 2011.
1229
1230 Stella, P., Kortner, M., Ammann, C., Foken, T., Meixner, F. X. and Trebs, I.: Measurements of
1231 nitrogen oxides and ozone fluxes by eddy covariance at a meadow: Evidence for an internal leaf
1232 resistance to NO₂, *Biogeosciences*, 10(9), 5997–6017, doi:10.5194/bg-10-5997-2013, 2013.
1233
1234 Sulman, B. N., Desai, A. R., Cook, B. D., Saliendra, N. and Mackay, D. S.: Contrasting carbon
1235 dioxide fluxes between a drying shrub wetland in Northern Wisconsin, USA, and nearby forests,
1236 *Biogeosciences*, 6(6), 1115–1126, doi:10.5194/bg-6-1115-2009, 2009.
1237
1238 Tai, A. P. K., Martin, M. V. and Heald, C. L.: Threat to future global food security from climate
1239 change and ozone air pollution, *Nat. Clim. Chang.*, 4, 817–821, doi:10.1038/nclimate2317, 2014.
1240
1241 Taylor, J. R.: *An Introduction to Error Analysis*, University Science Books, Sausalito., 1997.
1242
1243 Tedeschi, V., Ret, A., Manca, G., Valentini, R., Jarvis, P. G. and Borghetti, M.: Soil respiration
1244 in a Mediterranean oak forest at different developmental stages after coppicing, *Glob. Chang.*
1245 *Biol.*, 12(1), 110–121, doi:10.1111/j.1365-2486.2005.01081.x, 2006.

1246
1247 Thum, T., Aalto, T., Laurila, T., Aurela, M., Kolari, P. and Hari, P.: Parametrization of two
1248 photosynthesis models at the canopy scale in a northern boreal Scots pine forest, *Tellus B*, 59(5),
1249 doi:10.3402/tellusb.v59i5.17066, 2007.
1250
1251 UNECE: Revised manual on methodologies and criteria for mapping critical levels/loads and
1252 geographical areas where they are exceeded, in UNECE Convention on Long-range
1253 Transboundary Air Pollution., 2004.
1254
1255 Urbanski, S., Barford, C., Wofsy, S., Kucharik, C., Pyle, E., Budney, J., McKain, K., Fitzjarrald,
1256 D., Czikowsky, M. and Munger, J. W.: Factors controlling CO₂ exchange on timescales from
1257 hourly to decadal at Harvard Forest, *J. Geophys. Res.*, 112(G2), G02020,
1258 doi:10.1029/2006jg000293, 2007.
1259
1260 Valentini, R., Angelis, P., Matteucci, G., Monaco, R., Dore, S. and Mucnozza, G. E. S.: Seasonal
1261 net carbon dioxide exchange of a beech forest with the atmosphere, *Glob. Chang. Biol.*, 2(3),
1262 199–207, doi:10.1111/j.1365-2486.1996.tb00072.x, 1996.
1263
1264 Verma, S. B., Dobermann, A., Cassman, K. G., Walters, D. T., Knops, J. M., Arkebauer, T. J.,
1265 Suyker, A. E., Burba, G. G., Amos, B., Yang, H., Ginting, D., Hubbard, K. G., Gitelson, A. A.
1266 and Walter-Shea, E. A.: Annual carbon dioxide exchange in irrigated and rainfed maize-based
1267 agroecosystems, *Agric. For. Meteorol.*, 131(1–2), 77–96, doi:10.1016/j.agrformet.2005.05.003,
1268 2005.
1269
1270 Vitale, L., Tommasi, P. Di, D’Urso, G. and Magliulo, V.: The response of ecosystem carbon
1271 fluxes to LAI and environmental drivers in a maize crop grown in two contrasting seasons, *Int. J.*
1272 *Biometeorol.*, 60(3), 411–420, doi:10.1007/s00484-015-1038-2, 2015.
1273
1274 Vuichard, N. and Papale, D.: Filling the gaps in meteorological continuous data measured at
1275 FLUXNET sites with ERA-Interim reanalysis, *Earth Syst. Sci. Data*, 7(2), 157–171,
1276 doi:10.5194/essd-7-157-2015, 2015.
1277
1278 Van Der Walt, S., Colbert, S. C. and Varoquaux, G.: The NumPy array: A structure for efficient
1279 numerical computation, *Comput. Sci. Eng.*, 13(2), 22–30, doi:10.1109/MCSE.2011.37, 2011.
1280
1281 Wang, L., Good, S. P. and Caylor, K. K.: Global synthesis of vegetation control on
1282 evapotranspiration partitioning, *Geophys. Res. Lett.*, 41(19), 6753–6757,
1283 doi:10.1002/2014GL061439, 2014.
1284
1285 Warton, D. I., IJ, W., DS, F. and M, W.: Bivariate line-fitting methods for allometry, *Biol Rev*,
1286 81, 259–291, doi:10.1017/S1464793106007007, 2006.
1287
1288 Weaver, J. E. and Bruner, W. E.: Root development of vegetable crops, McGraw-Hill Book
1289 Company, Inc., Lincoln, Nebraska., 1927.
1290
1291 Wesely, M. L. and Hicks, B. B.: Some factors that affect the deposition rates of sulfur dioxide

1292 and similar gases on vegetation, *J. Air Pollut. Control Assoc.*, 27(11), 1110–1116,
1293 doi:10.1080/00022470.1977.10470534, 1977.

1294

1295 Wesley, M. L.: Parametrization of surface resistance to gaseous dry deposition in regional-scale
1296 numerical model, *Atmos. Environ.*, 23(6), 1293–1304, 1989.

1297

1298 Wittig, V. E., Ainsworth, E. A. and Long, S. P.: To what extent do current and projected
1299 increases in surface ozone affect photosynthesis and stomatal conductance of trees? A meta-
1300 analytic review of the last 3 decades of experiments, *Plant, Cell Environ.*, 30(9), 1150–1162,
1301 doi:10.1111/j.1365-3040.2007.01717.x, 2007.

1302

1303 Wittig, V. E., Ainsworth, E. A., Naidu, S. L., Karnosky, D. F. and Long, S. P.: Quantifying the
1304 impact of current and future tropospheric ozone on tree biomass, growth, physiology and
1305 biochemistry: A quantitative meta-analysis, *Glob. Chang. Biol.*, 15(2), 396–424,
1306 doi:10.1111/j.1365-2486.2008.01774.x, 2009.

1307

1308 Wohlfahrt, G., Hammerle, A., Haslwanger, A., Bahn, M., Tappeiner, U. and Cernusca, A.:
1309 Seasonal and inter-annual variability of the net ecosystem CO₂ exchange of a temperate
1310 mountain grassland: Effects of weather and management, *J. Geophys. Res.*, 113(D8), D08110,
1311 doi:10.1029/2007jd009286, 2008.

1312

1313 Wolfe, G. M., Thornton, J. A., McKay, M. and Goldstein, A. H.: and Physics Forest-atmosphere
1314 exchange of ozone : sensitivity to very reactive biogenic VOC emissions and implications for in-
1315 canopy photochemistry, 11(2007), 7875–7891, doi:10.5194/acp-11-7875-2011, 2011.

1316

1317 Wu, S., Mickley, L. J., Jacob, D. J., Logan, J. A., Yantosca, R. M. and Rind, D.: Why are there
1318 large differences between models in global budgets of tropospheric ozone?, *J. Geophys. Res.*
1319 *Atmos.*, 112, D05302, doi:10.1029/2006JD007801, 2007.

1320

1321 Wu, Z., Schwede, D. B., Vet, R., Walker, J. T., Shaw, M., Staebler, R. and Zhang, L.: Evaluation
1322 and intercomparison of five North American dry deposition algorithms at a mixed forest site, *J.*
1323 *Adv. Model. Earth Syst.*, 10, doi:10.1029/2017MS001231, 2018.

1324

1325 Young, P. J., Archibald, A. T., Bowman, K. W., Lamarque, J.-F., Naik, V., Stevenson, D. S.,
1326 Tilmes, S., Voulgarakis, A., Wild, O., Bergmann, D., Cameron-Smith, P., Cionni, I., Collins, W.
1327 J., Dalsøren, S. B., Doherty, R. M., Eyring, V., Faluvegi, G., Horowitz, L. W., Josse, B., Lee, Y.
1328 H., MacKenzie, I. A., Nagashima, T., Plummer, D. A., Righi, M., Rumbold, S. T., Skeie, R. B.,
1329 Shindell, D. T., Strode, S. A., Sudo, K., Szopa, S. and Zeng, G.: Pre-industrial to end 21st
1330 century projections of tropospheric ozone from the Atmospheric Chemistry and Climate Model
1331 Intercomparison Project (ACCMIP), *Atmos. Chem. Phys.*, 13(4), 2063–2090, doi:10.5194/acp-
1332 13-2063-2013, 2013.

1333

1334 Yue, X. and Unger, N.: Ozone vegetation damage effects on gross primary productivity in the
1335 United States, *Atmos. Chem. Phys.*, 14(17), 9137–9153, doi:10.5194/acp-14-9137-2014, 2014.

1336

1337 Yue, X., Keenan, T. F., Munger, W. and Unger, N.: Limited effect of ozone reductions on the

1338 20-year photosynthesis trend at Harvard forest, *Glob. Chang. Biol.*, 22(11), 3750–3759,
1339 doi:10.1111/gcb.13300, 2016.
1340
1341 Zeller, K. F. and Nikolov, N. T.: Quantifying simultaneous fluxes of ozone , carbon dioxide and
1342 water vapor above a subalpine forest ecosystem, *Environ. Pollut.*, 107, 1–20, 2000.
1343
1344 Zhang, L., Brook, J. R. and Vet, R.: On ozone dry deposition - With emphasis on non-stomatal
1345 uptake and wet canopies, *Atmos. Environ.*, 36(30), 4787–4799, doi:10.1016/S1352-
1346 2310(02)00567-8, 2002.
1347
1348 Zhang, L., Brook, J. R. and Vet, R.: A revised parameterization for gaseous dry deposition in air-
1349 quality models, *Atmos. Chem. Phys. Discuss.*, 3(2), 1777–1804, doi:10.5194/acpd-3-1777-2003,
1350 2003.
1351
1352 Zhang, Y. and Wang, Y.: Climate-driven ground-level ozone extreme in the fall over the
1353 Southeast United States, *Proc. Natl. Acad. Sci.*, 113(36), 201602563,
1354 doi:10.1073/pnas.1602563113, 2016.
1355
1356 Zhou, S., Yu, B., Huang, Y. and Wang, G.: Partitioning evapotranspiration based on the concept
1357 of underlying water use efficiency, *Water Resour. Res.*, 52, 1160–1175,
1358 doi:10.1002/2015WR017766., 2016.
1359
1360 Zielis, S., Etzold, S., Zweifel, R., Eugster, W., Haeni, M. and Buchmann, N.: NEP of a Swiss
1361 subalpine forest is significantly driven not only by current but also by previous years weather,
1362 *Biogeosciences*, 11(6), 1627–1635, doi:10.5194/bg-11-1627-2014, 2014.
1363
1364 Zona, D., Gioli, B., Fares, S., De Groot, T., Pilegaard, K., Ibrom, A. and Ceulemans, R.:
1365 Environmental controls on ozone fluxes in a poplar plantation in Western Europe, *Environ.*
1366 *Pollut.*, 184, 201–210, doi:10.1016/j.envpol.2013.08.032, 2014.
1367
1368

1369 Table 1. Description of sites that measure O₃ flux and their daytime growing season conditions ^a
 1370

	Blodgett Forest, California, USA	Hyytiälä Forest, Finland	Harvard Forest, Massachusetts, USA
Latitude, Longitude	38.8953, -120.6328	61.8475, 24.2950	42.5378, -72.1715
Plant functional type	Evergreen needleleaf	Evergreen needleleaf	Deciduous broadleaf
Years of data	2001-2007	2007-2012	1993-1999
Days of observations	1281	1098	1281
Canopy height, m	8	15	24
GPP, $\mu\text{mol m}^{-2} \text{s}^{-1}$	9.22 \pm 3.55	11.1 \pm 5.02	12.4 \pm 7.62
ET, $\text{mmol m}^{-2} \text{s}^{-1}$	3.25 \pm 1.23	1.71 \pm 0.82	2.95 \pm 1.70
PAR, $\mu\text{mol m}^{-2} \text{s}^{-1}$	875 \pm 149	690 \pm 203	876 \pm 222
Air Temperature, $^{\circ}\text{C}$	19.1 \pm 5.36	13.3 \pm 5.99	17.65 \pm 5.75
VPD, kPa	1.51 \pm 0.61	0.73 \pm 0.32	0.90 \pm 0.34
O ₃ , ppb	55.4 \pm 13.4	32.2 \pm 8.68	48.8 \pm 15.8
F_{s,O_3} , $\text{nmol O}_3 \text{m}^{-2} \text{s}^{-1}$	5.18 \pm 2.11	4.35 \pm 1.66	7.23 \pm 4.87
Precipitation, mm day^{-1}	0.09 \pm 0.49	0.42 \pm 0.89	0.28 \pm 0.82

1371
 1372 ^a Values are mean \pm standard deviation of daily averages, using daytime observations only. GPP is gross
 1373 primary productivity. ET is evapotranspiration. PAR is photosynthetically active radiation. VPD is vapor
 1374 pressure deficit. F_{s,O_3} is observation-derived stomatal O₃ flux.

1375
 1376
 1377
 1378 Table 2. Mean O₃ SynFlux, deposition velocity and its conductance components during daytime
 1379 in the growing season, grouped by plant functional type (PFT).^a
 1380

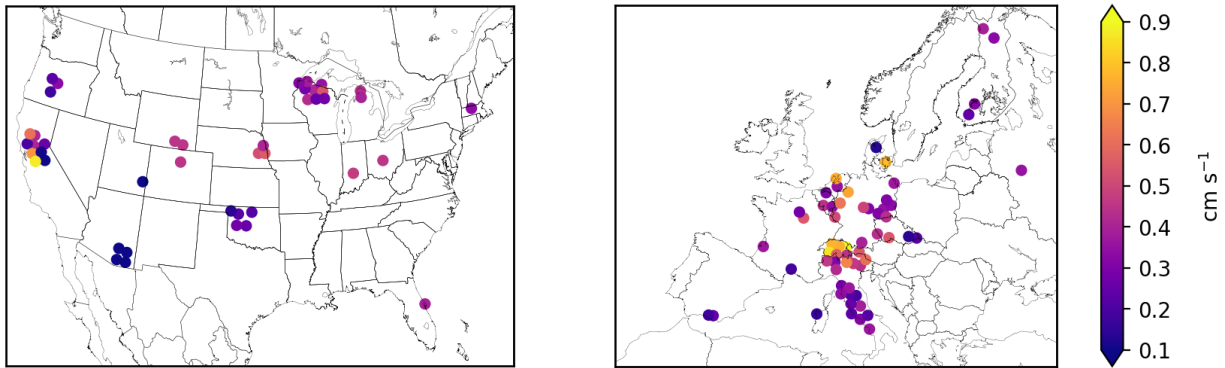
PFT ^b	Sites	Site- Years	g_s	g_{ns}	g_c	v_d	$F_{O_3}^{\text{syn}}$	F_{s,O_3}^{syn}	CUO	CUO3
CRO	18	148	0.42 \pm 0.17	0.28 \pm 0.09	0.68 \pm 0.18	0.53 \pm 0.12	7.66 \pm 1.96	4.77 \pm 1.52	24.8 \pm 12.4	14.9 \pm 9.3
ENF	25	254	0.37 \pm 0.10	0.25 \pm 0.06	0.60 \pm 0.11	0.54 \pm 0.10	7.37 \pm 1.33	4.61 \pm 1.16	20.0 \pm 5.69	11.9 \pm 6.30
EBF	3	31	0.21 \pm 0.02	0.15 \pm 0.02	0.36 \pm 0.03	0.33 \pm 0.03	5.02 \pm 0.65	2.90 \pm 0.28	12.1 \pm 0.81	5.12 \pm 0.45
DBF	16	158	0.41 \pm 0.14	0.20 \pm 0.09	0.60 \pm 0.18	0.53 \pm 0.15	7.87 \pm 2.28	5.37 \pm 1.69	28.6 \pm 13.8	15.7 \pm 6.66
MF	5	83	0.44 \pm 0.17	0.19 \pm 0.01	0.62 \pm 0.15	0.56 \pm 0.14	7.82 \pm 1.91	5.53 \pm 2.15	24.9 \pm 10.5	15.9 \pm 8.90
WSA	2	25	0.10 \pm 0.02	0.31 \pm 0.06	0.39 \pm 0.04	0.36 \pm 0.04	6.14 \pm 0.20	1.47 \pm 0.31	6.46 \pm 1.43	2.54 \pm 1.72
OSH	4	14	0.19 \pm 0.07	0.29 \pm 0.10	0.47 \pm 0.10	0.41 \pm 0.09	5.69 \pm 1.33	2.23 \pm 0.87	8.60 \pm 3.27	2.27 \pm 1.54
CSH	2	15	0.27 \pm 0.11	0.29 \pm 0.01	0.57 \pm 0.09	0.49 \pm 0.05	6.78 \pm 0.95	3.34 \pm 1.24	14.3 \pm 5.30	7.62 \pm 5.49
GRA	18	136	0.40 \pm 0.30	0.24 \pm 0.11	0.64 \pm 0.26	0.47 \pm 0.15	7.04 \pm 7.04	4.12 \pm 2.45	18.3 \pm 10.7	9.90 \pm 6.98
WET ^c	10	53	0.48 \pm 0.16	0.27 \pm 0.09	0.74 \pm 0.21	0.58 \pm 0.14	8.80 \pm 2.74	5.77 \pm 2.08	25.1 \pm 9.65	19.4 \pm 15.6

1381
 1382 ^a Values are the mean \pm standard deviation across sites within each PFT. Units are cm s^{-1} for g_s , g_{ns} , g_c ,
 1383 and v_d ; $\text{nmol O}_3 \text{m}^{-2} \text{s}^{-1}$ for $F_{O_3}^{\text{syn}}$ and F_{s,O_3}^{syn} ; and $\text{mmol O}_3 \text{m}^{-2}$ for CUO and CUO3.

1384 ^b CRO = crop, ENF = evergreen needleleaf forest, EBF = evergreen broadleaf forest, DBF = deciduous
 1385 broadleaf forest, MF = mixed forest, WSA = woody savanna, OSH = open shrubland, CSH = closed
 1386 shrubland, GRA = grassland, WET = wetland

1387 ^c Fluxes may be overestimated at wetland sites due to evaporation of surface water affecting the
 1388 calculation of g_s , but any errors are likely modest because the g_s values here are reasonable (Drake et al.,
 1389 2013).

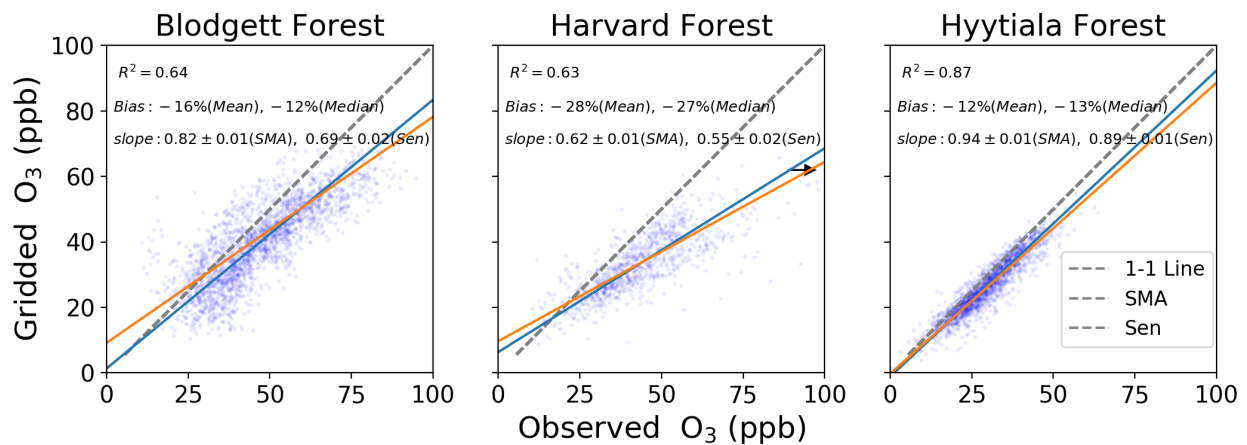
1390



1391
1392

1393 Figure 1. Mean stomatal conductance for O₃ (g_s) during daytime in the growing season at
 1394 FLUXNET2015 sites in the United States and Europe. Symbols of some sites have been moved
 1395 slightly to reduce overlap and improve legibility.

1396
1397

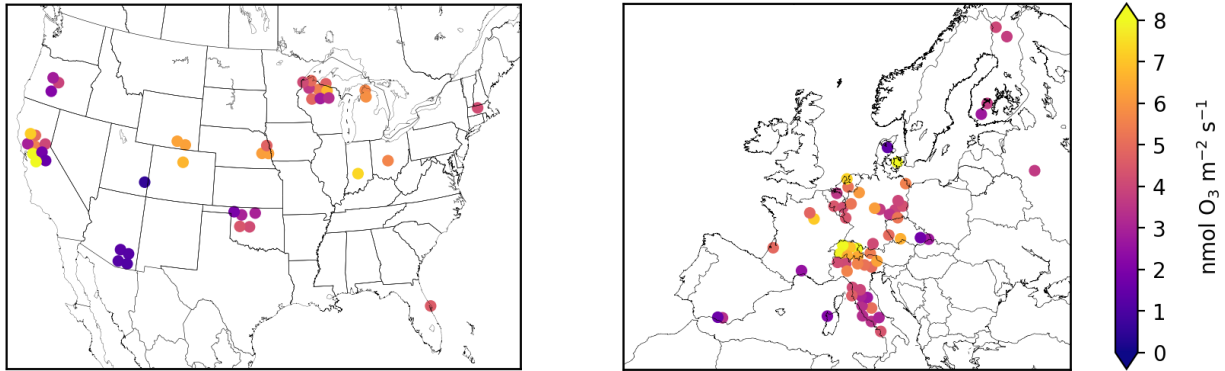


1398
1399

1400 Figure 2. Gridded and observed daily daytime O₃ concentrations at Blodgett, Harvard, and
 1401 Hyytiälä Forests. Inset numbers provide the coefficient of determination (R^2), mean and median
 1402 bias, the standard major axis (SMA) slope, the Thiel-Sen (Sen) slope, and the 68% confidence
 1403 interval of the slopes. Black arrow points towards outliers that are not shown.

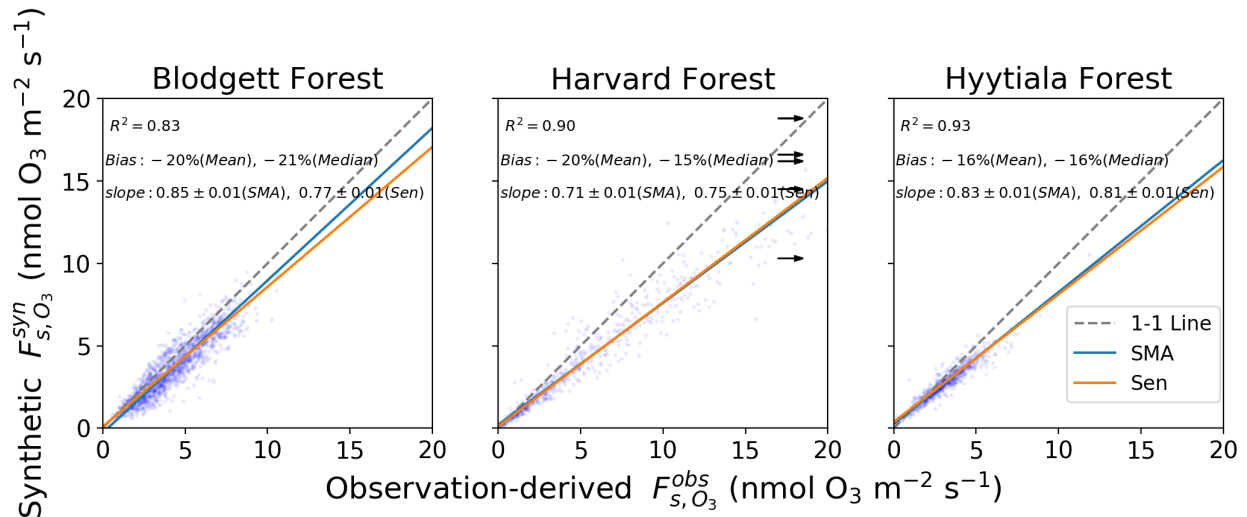
1404

1405



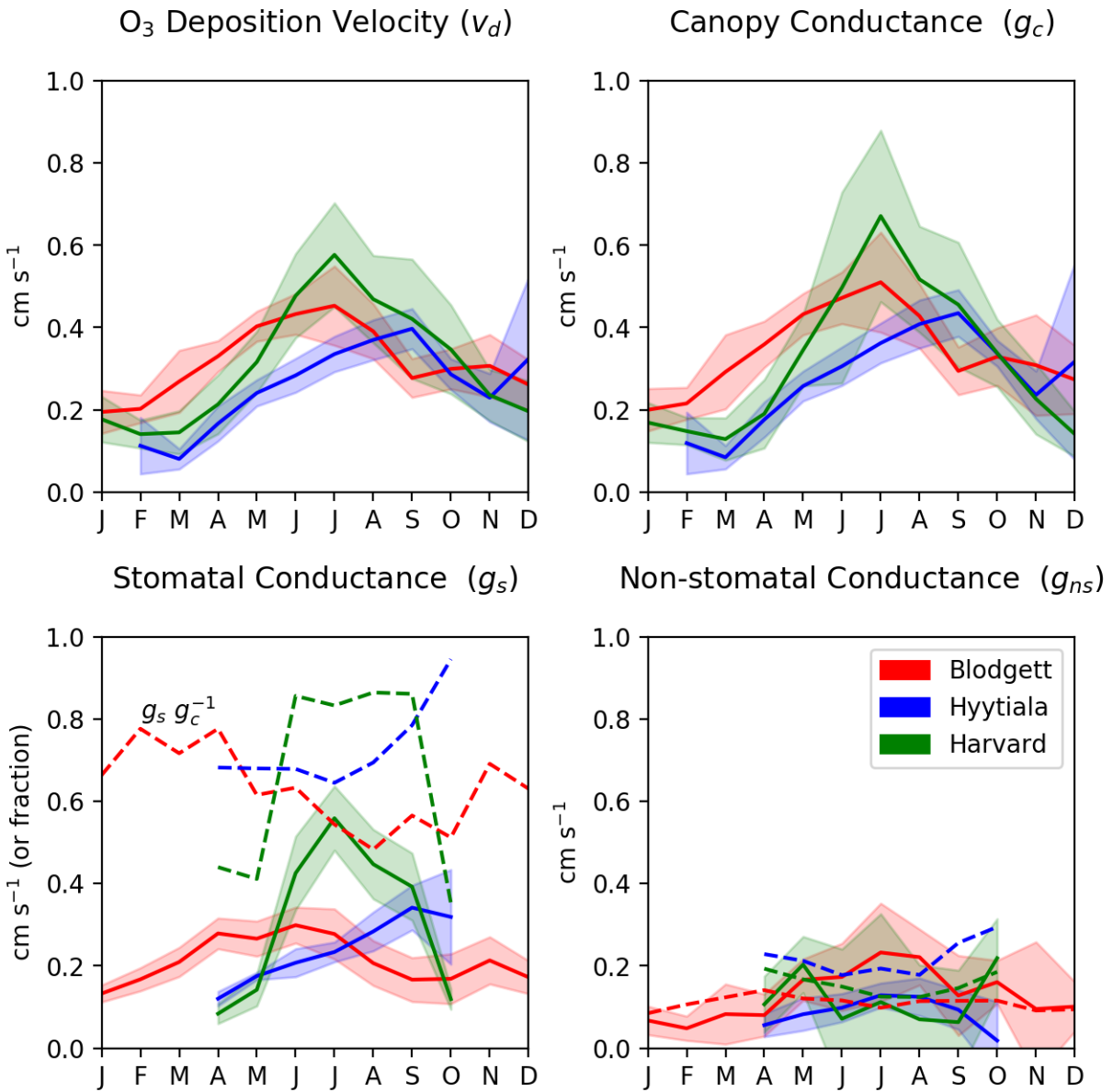
1406

1407 Figure 3. Mean synthetic stomatal O_3 flux (F_{s,O_3}^{syn} , Sect. 2.1) during the daytime growing season at
 1408 FLUXNET2015 sites in the United States and Europe. Symbols of some sites have been moved
 1409 slightly to reduce overlap and improve legibility.
 1410



1411

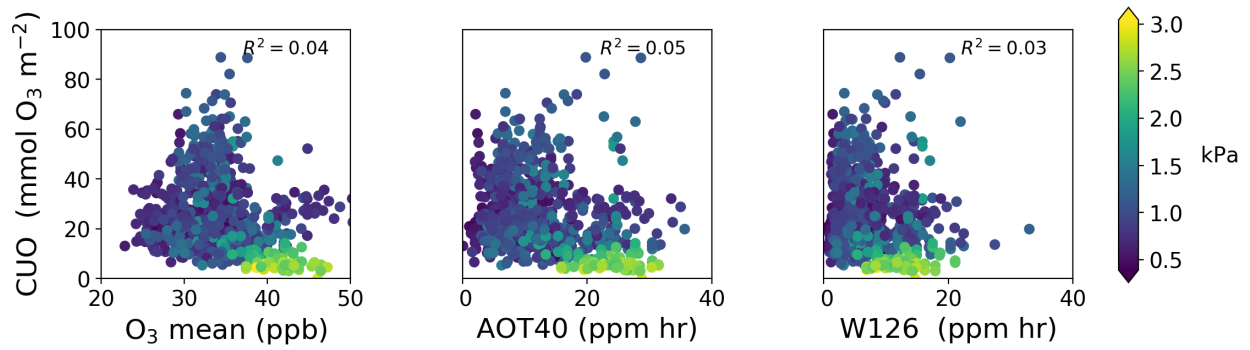
1412 Figure 4. Synthetic and observation-derived daily daytime stomatal O_3 flux. See Sect. 2.1 for
 1413 definition of F_{s,O_3}^{syn} and Fig. 2 for explanation of lines and inset text.



1414
 1415
 1416
 1417
 1418
 1419
 1420

Figure 5. Observed O_3 deposition velocity and its in-canopy components at sites with O_3 flux measurements. Lines show the multi-year mean and multi-year standard deviation calculated from the monthly averages described in Sect. 2.4. Dashed lines on the stomatal conductance panel show the stomatal fraction of total canopy conductance ($g_s g_c^{-1}$) and dashed lines on the non-stomatal conductance panel show the parameterized g_{ns} value.

1421



1422

1423

1424

1425

1426

1427

1428

Figure 6. Comparison of cumulative uptake of O₃ (CUO) to concentration-based metrics of O₃ exposure during the daytime growing season at 103 sites: mean O₃ concentration (left), AOT40 (center), and W126 (right). There is one value (dot) per site per year. Colors show mean vapor pressure deficit during the growing season.